Product and Ratio of Product of Fisher-Snedecor F Variates and Their Applications to Performance Evaluations of Wireless Communication Systems

Received October 29, 2020, accepted November 16, 2020, date of publication November 20, 2020,
date of current version December 10, 2020.

Digital Object Identifier 10.1109/ACCESS.2020.3039680

Product and Ratio of Product of Fisher-Snedecor $\mathcal{F}$ Variates and Their Applications to Performance Evaluations of Wireless Communication Systems

OSAMAH S. BADARNEH[1], (Member, IEEE), PASCHALIS C. SOFOTASIOS[2,3], (Senior Member, IEEE), SAMI MUHAIDAT[2,4], (Senior Member, IEEE), SIMON L. COTTON[5], (Senior Member, IEEE), AND DANIEL BENEVIDES DA COSTA[6], (Senior Member, IEEE)

[1]Electrical and Communication Engineering Department, School of Electrical Engineering and Information Technology, German-Jordanian University, Amman 11180, Jordan
[2]Center for Cyber-Physical Systems, Department of Electrical Engineering and Computer Science, Khalifa University, Abu Dhabi, United Arab Emirates
[3]Department of Electrical Engineering, Tampere University, 33101 Tampere, Finland
[4]Department of Systems and Computer Engineering, Carleton University, Ottawa, ON K1S 5B6, Canada
[5]Institute of Electronics, Communications and Information Technology, Queen's University Belfast, Belfast BT3 9DT, U.K.
[6]Department of Computer Engineering, Federal University of Ceará, Sobral 62010-560, Brazil

Corresponding author: Osamah S. Badarneh (osamah.badarneh@gju.edu.jo)

This work was supported in part by the Khalifa University under Grant KU/FSU-8474000122 and Grant KU/RC1-C2PS-T2/8474000137.

ABSTRACT This article considers the product, and the ratio of the product of Fisher-Snedecor $\mathcal{F}$ random variables (RVs), which can be used in modeling fading conditions that are encountered in realistic wireless transmission. To this end, exact analytical expressions are derived for the probability density function (PDF) and cumulative distribution function (CDF) of the product of N statistically independent, but not necessarily identically distributed, Fisher-Snedecor $\mathcal{F}$ RVs. Capitalizing on these, exact analytical expressions are then derived for the outage probability, average channel capacity and average bit error probability over cascaded fading channels. Moreover, some important statistical metrics such as amount of fading, channel quality estimation index, kurtosis, and skewness are also provided, since they provide useful insights on the characteristics of the encountered fading conditions. In addition, with the aid of the central limit theorem, an approximation for the PDF of $N*$Fisher-Snedecor $\mathcal{F}$ RVs is proposed using a lognormal density, and its accuracy is quantified in terms of the resistor-average distance. Finally, novel expressions for the PDF and CDF of the N-fold product ratio of Fisher-Snedecor $\mathcal{F}$ RVs are also derived. As a potential application of our new results, a spectrum sharing network is considered, for which exact analytical expressions for the outage probability, delay-limited capacity, and ergodic capacity are derived. For the cascaded fading scenario and the spectrum sharing network, numerical examples are provided to show the impact of different channel-related parameters, such as fading severity, shadowing, peak and average interference power on the system performance, which is rather useful in the design of conventional and emerging wireless communication systems. Monte-Carlo simulation results are provided to corroborate the presented mathematical analysis.

INDEX TERMS Cascaded channels, cognitive radio, fading, $\mathcal{F}$ distribution, shadowing, spectrum sharing.

I. INTRODUCTION

Multipath fading and shadowing are two of the most significant factors, which must be taken into account when characterizing wireless communication channels [2]. Throughout the literature, a number of models can be found which are used to characterize multipath fading such as the Nakagami-m and Rice fading models, and more recently the κ-μ, η-μ, and α-μ fading models [3]–[5]. Similarly, there are a number of different statistical distributions which aim to model the shadowing phenomena including the lognormal distribution, which is often approximated by the gamma

The associate editor coordinating the review of this manuscript and approving it for publication was Adao Silva.

distribution owing to its mathematical tractability [2]. Combining the simultaneous effects of fading[1] and shadowing, has led to the creation of a range of so-called composite fading distributions, which are particularly useful in accounting for the simultaneous occurrence of multipath fading and shadowing during wireless transmission. Some well-known composite fading models in the open technical literature are the K-distribution, κ-μ shadowed, κ-μ/gamma, η-μ/gamma, and α-μ/gamma, κ-μ/inverse gamma, η-μ/inverse gamma, and extended generalized-K (EGK) distributions, which can be found in [6]–[20]. However, while these composite models may characterize the underlying fading phenomena in a reasonably accurate manner, quite often their mathematical representation leads to cumbersome, if not intractable, analytic results for most important performance measures of interest. This unfortunately impacts the formulation of critical statistical metrics such as the probability density function (PDF), the cumulative distribution function (CDF), and the moment generating function (MGF), which are required to evaluate important performance metrics such as the bit/symbol error probability, channel capacity, and outage probability (OP).

Over the years, significant effort has been devoted to evaluating the performance of both multipath fading and composite fading models in different communication scenarios [1], [21]–[42] and the references therein. In this context, the authors in [21] introduced a rather general product distribution known as $N*$Nakagami-m. This distribution arises as a result of the product of N statistically independent, but not necessarily identically distributed (i.n.i.d.), Nakagami-m random variables (RVs), which has been shown to provide accurate characterization of fading conditions during realistic wireless transmission. Subsequently, Trigui *et al.* introduced a distribution referred to as $N*$generalized-K, which is constructed as the product of N statistically i.n.i.d. generalized-K RVs [22]. Likewise, the authors in [23] developed the $N*$generalized Nakagami-m (GNM) distribution ($N*$GNM distribution), which is constructed as the product of N statistically i.n.i.d. GNM RVs. In [24], the authors introduced a stochastic fading channel model called cascaded Weibull fading, which was generated through the product of i.n.i.d. Weibull RVs. Based on these contributions, the performance of multihop-intervehicular communication systems with regenerative and non-regenerative relaying over $N*$Rayleigh fading channels was investigated in [25]. In [26], the authors analyzed the OP performance of single carrier and multi-carrier systems over $N*$Nakagami-m fading channels in the presence of in-phase/quadrature-phase imbalances at the front end of the receiver. The product of N i.n.i.d. squared generalized-K (KG) RVs is considered in [27], while recently, some important statistical metrics of the double-generalized Gamma distribution such as the joint PDF, CDF, and MGF were derived in simplified forms in [28]. These metrics were then employed to analyze the performance of a transmit antenna selection system operating in vehicle-to-vehicle communications [28].

In the same context, the PDF and CDF of the ratio of two i.n.i.d. α-μ RVs [5] and their applications in spectrum sharing networks were reported in [29]. Finally, in [30], the performance of the product of two i.n.i.d. α-μ (so-called α-μ/α-μ) distributions were analyzed and new relationships between the α-μ/α-μ distribution and the EGK distribution were developed in [13]. It is recalled that the product and ratio of products of RVs are of great importance in wireless communication theory as they find application in a broad range of wireless communication systems. Typical examples include wireless transmission in cascaded fading channels [21], [43]–[46], in keyhole channels of multiple-input multiple-output (MIMO) systems [47] and in multi-hop communication systems [48], where the received signal is treated as a product of RVs. Also, in backscatter communications such as those found in radio frequency identification (RFID) systems, the channel between the reader and the tag and likewise, between the tag and the reader can be modeled as a product of RVs [49]–[52]. Additionally, the product of two RVs can be used to model high resolution synthetic aperture radar clutter [53]. On the other hand, the ratio of products of RVs finds application in the aforementioned scenarios when modeling the statistics of some quantities such as the signal-to-interference ratio (SIR) [54]–[59], e.g., cognitive radio networks [29]. In addition, the ratio of products of RVs finds application in modeling the statistics of composite fading channels.

Recently, a new composite fading distribution, known as the Fisher-Snedecor $\mathcal{F}$ distribution, was proposed in [60]. In this composite fading model, the scattered multipath fading follows a Nakagami-m distribution, while the root-mean-square (rms) signal is weighted by an inverse Nakagami-m RV. Through versatile measurement campaigns in realistic communication scenarios, this composite model was shown to provide accurate characterization of multipath fading and shadowing conditions in various realistic communication scenarios. In addition, its algebraic representation is relatively simple, which renders it convenient to handle both analytically and numerically. Nevertheless, despite the importance of this composite model, the product and the ratio of the product of this type of variable have not been addressed. Motivated by this, in the present paper, some important statistics of the product and ratio of product of Fisher-Snedecor $\mathcal{F}$ RVs such as the PDF, and CDF are derived. Due to their fundamental nature, these results will be useful in many areas of mathematical and statistical research. Specifically, the contributions of this work are summarized below:

- For the product of Fisher-Snedecor $\mathcal{F}$ RVs:
  - Novel exact analytical expressions for the PDF and CDF are derived. These expressions include the well-known Nakagami-m and Rayleigh distributions as special cases.
  - The derived statistics are employed to analyze the performance of cascaded fading channels.

[1] Herein fading refers to multipath fading whereas shadowing refers to the shadowed fading.

  - Novel exact analytical expressions for the OP, average bit error probability (BEP), and ergodic capacity are derived and evaluated.
  - Some important statistical metrics such as the amount of fading (AoF), channel quality estimation index (CQEI), kurtosis, and skewness are obtained in closed-form.
  - Motivated by the central limit theorem (CLT), an approximation for the PDF of $N*$Fisher-Snedecor $\mathcal{F}$ RVs is constructed using a lognormal density. The accuracy of the approximated PDF is quantified extensively in terms the resistor-average distance (RAD).
- For the ratio of the product:
  - Exact analytical expressions for the PDF and CDF are derived.
  - As a potential application, the analysis of a spectrum sharing network is considered. To this end, novel analytical expressions for the OP (or outage capacity), delay-limited capacity, and ergodic capacity are derived.

To validate the work presented here, the obtained expressions for both the cascaded system and the spectrum sharing network are numerically evaluated and compared with respective results from Monte-Carlo simulations. Very good agreement is observed across all ranges of the results, consolidating our mathematical framework. Also, the offered results lead to numerous insights that are expected to be useful in the design and robust operation of emerging wireless communication systems.

The remainder of this article is organized as follows. Section II introduces some preliminary information related to the Fisher-Snedecor $\mathcal{F}$ composite fading model which are essential for the subsequent derivation of the analytic results. Section III derives some statistics of the product of Fisher-Snedecor $\mathcal{F}$ RVs, while Section IV illustrates some practical scenarios of interest in which the product of RVs finds applicability. In Section V, a performance analysis of Fisher-Snedecor $\mathcal{F}$ cascaded fading channels is thoroughly conducted. Section VI investigates the necessary conditions for the cascaded Fisher-Snedecor $\mathcal{F}$ fading distribution to be accurately approximated by a lognormal distribution. Considering the ratio of the product of Fisher-Snedecor $\mathcal{F}$ RVs, Section VII derives some useful statistics, while Section VIII makes use of the derived expressions to analyze the performance of a spectrum sharing network. Numerical examples and simulation results are then provided in Section IX, while, Section X concludes this article with some closing remarks.

II. PRELIMINARIES

In a Fisher-Snedecor $\mathcal{F}$ fading channel, the received signal envelope, R_ℓ, is given by

$$R_\ell^2 = \sum_{n=1}^{m_\ell} A^2 I_n^2 + A^2 Q_n^2 \tag{1}$$

in which m_ℓ represents the number of separable clusters of multipath, where the scattered waves have similar delay times, with the delay spreads of different clusters being relatively large. Additionally, the rms power of the received signal experiences random variations induced by shadowing. I_n and Q_n are independent Gaussian RVs which represent the in-phase and quadrature phase components of the cluster n, with $\mathbb{E}[I_n] = \mathbb{E}[Q_n] = 0$ and $\mathbb{E}[I_n^2] = \mathbb{E}[Q_n^2] = \sigma^2$, and $\mathbb{E}[\cdot]$ denoting the expectation operator. In (1), A represents a normalized inverse Nakagami-m RV, with $\mathbb{E}[A^2] = 1$, where its PDF is given by [61]

$$f_A(\alpha) = \frac{2(m_{s_\ell} - 1)^{m_{s_\ell}}}{\Gamma(m_{s_\ell})\alpha^{2m_{s_\ell}+1}} e^{-\frac{m_{s_\ell}-1}{\alpha^2}} \tag{2}$$

in which m_{s_ℓ} is the scale parameter of the distribution. Based on (2) and with the help of the analysis in [60], the PDF of the received signal envelope of the Fisher-Snedecor $\mathcal{F}$ fading distribution can be derived as [61]

$$f_{R_\ell}(r) = \frac{2m_\ell^{m_\ell}((m_{s_\ell} - 1)\Omega_\ell)^{m_{s_\ell}} r^{2m_\ell - 1}}{B(m_\ell, m_{s_\ell})\left(m_\ell r^2 + (m_{s_\ell} - 1)\Omega_\ell\right)^{m_\ell + m_{s_\ell}}}, \tag{3}$$

which is valid for $m_{s_\ell} > 1$. It is worth highlighting that (3) models multipath fading as a Nakagami-m process and shadowing as an inverse Nakagami-m process. In this model, m_ℓ represents the fading severity (equivalently, number of multipath clusters) and m_{s_ℓ} represents the shadowing parameter, $\Omega_\ell = \mathbb{E}[r^2]$ is the mean power, and $B(\cdot, \cdot)$ is the beta function [62, Eq. (8.384.1)]. It is noted that when $m_{s_\ell} \to \infty$, the PDF in (3) reduces to the Nakagami-m distribution and subsequently to the Rayleigh ($m_\ell = 1$) and one-sided Gaussian ($m_\ell = 1/2$) distributions.

Next, some preliminary results that assist in the analysis of different performance metrics such as OP, bit/symbol error probability, and channel capacity are provided. To this end, it is recalled that the Meijer's G-function is defined in terms of a Mellin-Barnes type integral [62, Eq. (9.301)],[2] that is

$$\begin{aligned} &\mathrm{G}_{p,q}^{u,n}\left[z \middle| \begin{matrix} a_1, a_2, \ldots, a_p \\ b_1, b_2, \ldots, b_q \end{matrix}\right] \\ &= \times \frac{1}{2\pi j} \oint_{\mathcal{L}} \frac{\prod_{i=1}^{u} \Gamma(b_i + s) \prod_{i=1}^{n} \Gamma(1 - a_i - s)}{\prod_{i=u+1}^{q} \Gamma(1 - b_i - s) \prod_{i=n+1}^{p} \Gamma(a_i + s)} z^{-s} ds, \end{aligned} \tag{4}$$

in which $0 \le u \le q$, $0 \le n \le p$, a_i and b_i may be complex. The contour $\mathcal{L}$ can be of three kinds: $\mathcal{L}_{-\infty}$, $\mathcal{L}_{+\infty}$, and $\mathcal{L}_{j\infty}$. The contour $\mathcal{L}_{-\infty}$ (or $\mathcal{L}_{+\infty}$) is the left (or right) begins in the

[2]The conditions under which the integral in (4) converges are listed in [62, Eq. (9.302)]. It is straightforward to show that the parameters of the Meijer's G-function in all equations satisfy these sufficient conditions, and therefore the Meijer's G-function converges.

point of $-\infty + jc$ $(+\infty + jc)$ such that all poles $s = -b_i - \ell, i = 1, \ldots, u, \ell = 0, 1, 2, \ldots$, of the integrand function at the left and all poles of $s = 1 - a_i + \ell, i = 1, \ldots, n, \ell = 0, 1, 2, \ldots$, at the right of the contour and at last $\mathcal{L}$ finishes in the point $-\infty + j\delta$ $(+\infty + j\delta)$, where $c < \delta$. The contour $\mathcal{L}_{j\infty}$ begins at the point $d - j\infty$ and finishes at the point $d + j\infty$, and separates the poles in the same way as $\mathcal{L}_{\pm\infty}$. It is noted that the Meijer's G-function is a standard built-in function in most of the well-known mathematical software packages such as Matlab, Maple, and Mathematica.

It is worth highlighting that when $b_i \to \infty$ the Meijer's G-function in (4) reduces to [63, Eq. (8.2.2.12)]

$$\lim_{|b_i|\to\infty} \frac{1}{\Gamma(b_i)} \mathrm{G}_{p,q}^{m,n}\left[b_i x \middle| \begin{matrix} a_1, a_2, \ldots, a_p \\ b_i, b_m, \ldots, b_q \end{matrix}\right] = \mathrm{G}_{p,q-1}^{m-1,n}\left[x \middle| \begin{matrix} a_1, a_2, \ldots, a_p \\ b_m, b_{m+1}, \ldots, b_q \end{matrix}\right]. \quad (5)$$

III. PRODUCTS OF FISHER-SNEDECOR $\mathcal{F}$ VARIATES

In what follows, the above results are employed in the derivation of the product and the ratio of the product of Fisher-Snedecor $\mathcal{F}$ variates.

Definition 1 (N∗Fisher-Snedecor $\mathcal{F}$ distribution): The distribution of the product, X, of N i.n.i.d. Fisher-Snedecor $\mathcal{F}$ RVs R_ℓ, for $1 \le \ell \le N$, $R_\ell \sim \mathcal{F}(m_\ell, m_{s_\ell}, \Omega_\ell)$, i.e.,

$$X \triangleq \prod_{\ell=1}^{N} R_\ell. \quad (6)$$

is defined as N∗Fisher-Snedecor $\mathcal{F}$ distribution, where the parameters m_ℓ $(0.5 \le m_\ell < \infty)$, m_{s_ℓ} $(1 < m_{s_\ell} < \infty)$, Ω_ℓ $(0 \le \Omega_\ell < \infty)$ are defined above, and $N \in \mathbb{R}^+$.

Theorem 1 (Moments): For $k \in \mathbb{R}^+$, the k-th order moment $\mathbb{E}[X^k]$ of X is given by

$$\mathbb{E}[X^k] = \prod_{\ell=1}^{N} \frac{\left(\frac{m_\ell}{(m_{s_\ell}-1)\Omega_\ell}\right)^{-\frac{1}{2}k}}{B(m_\ell, m_{s_\ell})} B\left(m_\ell + \frac{1}{2}k, m_{s_\ell} - \frac{1}{2}k\right). \quad (7)$$

Proof: The k-th order moment of X around the origin can be found using

$$\mathbb{E}[X^k] = \prod_{\ell=1}^{N} \mathbb{E}[R_\ell^k] = \prod_{\ell=1}^{N} \int_0^\infty r^k f_{R_\ell}(r) dr. \quad (8)$$

By, substituting (3) into (8) and with the aid of [62, Eq. (3.194.3)], the s-th moment of X is obtained. ∎

Theorem 2 (Probability Density Function): The PDF of X is given by (9)*, at the bottom of the next page.*

Proof: The PDF of X in (6) can be formulated as an inverse Mellin-Barnes transform [64], that is

$$f_X(x) = \frac{1}{x}\frac{1}{2\pi j} \oint_{\mathcal{L}} \mathbb{E}[X^s] x^{-s} ds, \quad (10)$$

in which $\mathcal{L}$ is an appropriate contour.

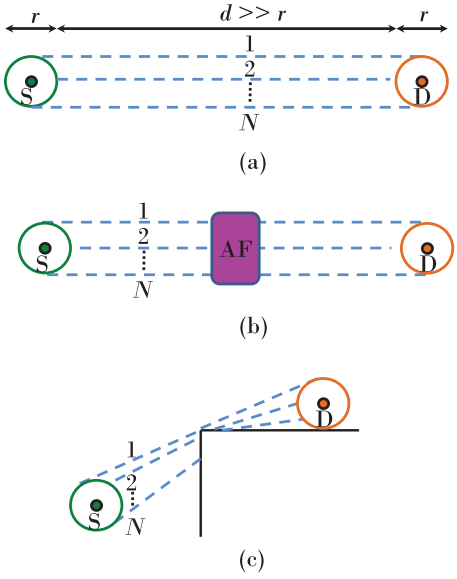

FIGURE 1. Some cascaded fading channel scenarios: (a) Keyhole, (b) amplify-and-forward relay and (c) diffraction.

Plugging (7) into (10), using [62, Eq. (8.384.1)], and after some mathematical manipulations, the PDF of X can be rewritten as

$$f_X(x) = \frac{1}{\prod_{\ell=1}^{N}\Gamma(m_\ell)\Gamma(m_{s_\ell})}\frac{1}{x}\frac{1}{2\pi j}\oint_{\mathcal{L}} x^{-s} \times \prod_{\ell=1}^{N}\Gamma(m_\ell + 0.5s)\Gamma(m_{s_\ell} - 0.5s)\left(\frac{m_\ell}{(m_{s_\ell}-1)\Omega_\ell}\right)^{-\frac{1}{2}s} ds. \quad (11)$$

After making the change of variable $t = \frac{1}{2}s$ in (11) and with the help of (4), the PDF of X is obtained.

Note that when $m_{s_\ell} \to \infty$, with the aid of [63, Eq. (8.2.2.14)], and applying an N-fold limit operation using (5), the PDF in (9) reduces to the PDF of the N∗Nakagami-m distribution given in [21, Eq. (4)]. ∎

Corollary 1 (Cumulative Distribution Function): The CDF of X can be derived as in (12), at the bottom of the next page.

Proof: Using (9) and [63, Eq. (2.24.2.2)], the CDF of X is attained. It is noted that when $m_{s_\ell} \to \infty$, (12) reduces to the CDF of the N∗Nakagami-m distribution given in [21, Eq. (7)]. ∎

IV. CASCADED FADING CHANNELS

In practical communication scenarios, there are cases that exhibit cascaded fading conditions. Some of these scenarios are depicted in Fig. 1 [65], [66]. Specifically, in the first scenario, Fig. 1(a), when the source node S and the destination node D are separated by a large distance ($d \gg \hat{d}$, where $\hat{d}$ represents the scatter ring diameter) and surrounded by many moving and stationary obstacles, the transmitted signal can

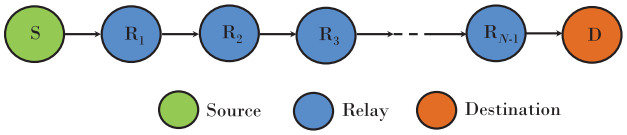

FIGURE 2. Cascaded fading channels constructed by AF-relay nodes.

propagate only through an electromagnetically small aperture, known as a keyhole. The keyhole acts as a source node to the subsequent keyholes, and therefore, the overall communication channel can be considered as a cascaded fading channel. In the same context, Fig. 1(b) shows the propagation in amplify-and-forward (AF) wireless relay networks. It is noted here that an AF relay node is essentially a keyhole [67]. As such, the received signal at the relay node is forwarded to the next relay node until the transmitted signal reaches its destination node. Finally, Fig. 1(c) illustrates propagation via diffracting edges, such as rooftops or street corners. The rooftop or the street corner essentially act as multipliers for a large number of statistically independent diffracted rays.

V. PERFORMANCE ANALYSIS OF CASCADED FADING CHANNELS

Consider a digital communication system that operates over an $N*$Fisher-Snedecor $\mathcal{F}$ fading channel and in the presence of additive white Gaussian noise (AWGN). In this system, the source node S and the destination node D are located far apart and cannot communicate with each other directly due to some constrains such as power constraints and channel fading effects. In this case, and without loss of generality, the communication can be established through multiple AF-relay nodes, as shown in Fig. 2. The information signal generated by the source node is sent to the next relay node, i.e., $\mathbb{R}_1$. Then, from the relay node $\mathbb{R}_1$, to the next relay node $\mathbb{R}_2$. This process continues until the information signal reaches the destination node D. Note that the relay nodes act as non-regenerative relays. This type of relaying only multiplies the received signal from the previous relay node by a constant gain determined by the path-loss, then retransmits the message without any type of signal processing. The transmission and reception are carried out in the same frequency band.

The instantaneous signal-to-noise ratio (SNR) per symbol at the receiver's antenna is given by:

$$\Gamma = \left(\frac{E_s}{N_0}\right) X^2, \tag{13}$$

in which E_s and N_0 represent the average transmitted energy per symbol and the single-sided AWGN, respectively. Based on this, the corresponding average SNR can be expressed as

$$\bar{\gamma} = \left(\frac{E_s}{N_0}\right) \mathbb{E}[X^2] = \left(\frac{E_s}{N_0}\right) \prod_{\ell=1}^{N} \Omega_\ell. \tag{14}$$

Corollary 2 (Probability Density Function): The PDF of the instantaneous SNR Γ is given by

$$f_\Gamma(\gamma) = \frac{\gamma^{-1}}{\prod_{\ell=1}^{N} \Gamma(m_\ell)\Gamma(m_{s_\ell})} \mathrm{G}_{N,N}^{N,N}\left[\frac{\gamma}{\bar{\gamma}} \prod_{\ell=1}^{N} \frac{m_\ell}{(m_{s_\ell}-1)} \middle| \begin{matrix} 1-m_{s_1}, 1-m_{s_2}, \ldots, 1-m_{s_N} \\ m_1, m_2, \ldots, m_N \end{matrix}\right]. \tag{15}$$

Proof: After performing a simple transformation of RVs with the aid of (13) and (14), the PDF of Γ can be obtained via [2]

$$f_\Gamma(\gamma) = \frac{f_X\left(\sqrt{\frac{\gamma}{\bar{\gamma}} \prod_{\ell=1}^{N} \Omega_\ell}\right)}{2\sqrt{\frac{\gamma\bar{\gamma}}{\prod_{\ell=1}^{N} \Omega_\ell}}}, \tag{16}$$

in which $f_X(\cdot)$ is defined in (9). Thus, the proof is completed. ■

Corollary 3 (Cumulative Distribution Function): The CDF of the instantaneous SNR Γ can be expressed as in (17), at the bottom of the next page.

Proof: After performing a simple transformation of RVs with the aid of (13) and (14), the CDF of Γ can be obtained via

$$F_\Gamma(\gamma) = F_X\left(\sqrt{\frac{\gamma}{\bar{\gamma}} \prod_{\ell=1}^{N} \Omega_\ell}\right), \tag{18}$$

in which $F_X(\cdot)$ is defined in (12). This completes the proof. ■

Corollary 4 (Moments): For $k \in \mathbb{R}^+$, the k-th moment of the instantaneous SNR Γ is given by

$$\mu_k = \mathbb{E}[\Gamma^k] = \bar{\gamma}^k \prod_{\ell=1}^{N} \frac{\Gamma(m_\ell + k)\Gamma(m_{s_\ell} - k)}{\Gamma(m_\ell)\Gamma(m_{s_\ell})} \left(\frac{m_{s_\ell} - 1}{m_\ell}\right)^k. \tag{19}$$

$$f_X(x) = \frac{2}{\prod_{\ell=1}^{N} \Gamma(m_\ell)\Gamma(m_{s_\ell})} x^{-1} \mathrm{G}_{N,N}^{N,N}\left[x^2 \prod_{\ell=1}^{N} \left(\frac{m_\ell}{(m_{s_\ell}-1)\Omega_\ell}\right) \middle| \begin{matrix} 1-m_{s_1}, 1-m_{s_2}, \ldots, 1-m_{s_N} \\ m_1, m_2, \ldots, m_N \end{matrix}\right]. \tag{9}$$

$$F_X(x) = \frac{\mathrm{G}_{N+1,N+1}^{N,N+1}\left[x^2 \prod_{\ell=1}^{N} \frac{m_\ell}{(m_{s_\ell}-1)\Omega_\ell} \middle| \begin{matrix} 1-m_{s_1}, 1-m_{s_2}, \ldots, 1-m_{s_N}, 1 \\ m_1, m_2, \ldots, m_N, 0 \end{matrix}\right]}{\prod_{\ell=1}^{N} \Gamma(m_\ell)\Gamma(m_{s_\ell})}. \tag{12}$$

Proof: Using (15) and [63, Eq. (2.24.2.1)], then (19) is obtained, which completes the proof. ■

A. AMOUNT OF FADING

The amount of fading (AoF) is a useful performance metric which can be used in the analysis of wireless communication systems. It is defined as the ratio of the variance to the square average of the instantaneous SNR and can be written as

$$\text{AoF} \triangleq \frac{Var(\Gamma)}{(\mathbb{E}[\Gamma])^2} = \frac{\mathbb{E}[\Gamma^2] - (\mathbb{E}[\Gamma])^2}{\bar{\gamma}^2}. \tag{20}$$

Using (19), the following simple expression is deduced for the AoF for the case of Fisher-Snedecor $\mathcal{F}$ fading channels

$$\text{AoF} = \prod_{\ell=1}^{N} \frac{\left(1+\frac{1}{m_\ell}\right)\left(1-\frac{1}{m_{s_\ell}}\right)}{\left(1-\frac{2}{m_{s_\ell}}\right)} - 1, \tag{21}$$

which reduces to the Nakagami-m case [21, Eq. (16)], when $m_{s_\ell} \to \infty$. It is evident from the derived expression that the AoF is a function only of the fading parameters and does not depend on the average SNR.

B. CHANNEL QUALITY ESTIMATION INDEX

The channel quality estimation index (CQEI) is defined as the ratio of the variance of the instantaneous received SNR Γ to the cubed mean of the received SNR Γ [68], that is

$$\text{CQEI} = \frac{Var[\Gamma]}{(\mathbb{E}[\Gamma])^3} = \frac{\text{AoF}}{\mathbb{E}[\Gamma]}. \tag{22}$$

With the help of (21), (22) is given as[3]

$$\text{CQEI} = \frac{1}{\bar{\gamma}} \left\{ \prod_{\ell=1}^{N} \frac{\left(1+\frac{1}{m_\ell}\right)\left(1-\frac{1}{m_{s_\ell}}\right)}{\left(1-\frac{2}{m_{s_\ell}}\right)} - 1 \right\}. \tag{23}$$

Table 1 lists the values of the AoF and CQEI metrics for $m = 3, m_s = 3$, and for different values of the average SNR $\bar{\gamma}$. It is noted that unlike the AoF metric, the CQEI provides useful insights on the effect of different values of the average SNR $\bar{\gamma}$.

C. KURTOSIS

Higher order statistics (HOS) performance metrics such as kurtosis and skewness can effectively lead to reliable communication designs. In [69], the aforementioned performance metrics are effectively used for the best channel selection in heterogeneous wireless networks with spectrum sharing and/or aggregation capabilities. The authors in [70], used these metrics to analyze vehicle-to-vehicle (V2V) communications in small-scale fading channels. Threshold selection methods for time of arrival (ToA) estimation in ultra-wide band (UWB) and 60 GHz communications based on kurtosis and Skewness were proposed in [71], [72], respectively.

[3] m and m_ℓ are used interchangeably. This holds also for m_s and m_{s_ℓ}.

TABLE 1. Values of AoF and CQEI for Different Values of N and $\bar{\gamma}$ with $m = 3$ and $m_s = 3$.

Metric	N	Average SNR $\bar{\gamma}$ (dB)				
		0	5	10	15	20
AoF	2	6.11	6.11	6.11	6.11	6.11
	4	49.57	49.57	49.57	49.57	49.57
	6	358.59	358.59	358.59	358.59	358.59
	8	2556.11	2556.11	2556.11	2556.11	2556.11
	10	18182.91	18182.91	18182.91	18182.91	18182.91
CQEI	2	6.11	1.93	0.61	0.19	0.06
	4	49.57	15.67	4.96	1.57	0.50
	6	358.59	113.40	35.86	11.34	3.59
	8	2556.11	808.31	255.61	80.83	25.56
	10	18182.91	5749.94	1818.29	574.99	181.83

It is recalled that kurtosis in statistics is used to measure the relative (i.e., relative to Gaussian distribution) peakedness or flatness of a distribution. Kurtosis can be defined as [73]

$$\begin{aligned} K_r &= \frac{\mathbb{E}\left[(\Gamma - \mathbb{E}[\Gamma])^4\right]}{\left(\mathbb{E}[\Gamma^2] - \mathbb{E}^2[\Gamma]\right)^2} - 3 \\ &= \frac{\mu_4 - 4\mu_1\mu_3 + 6\mu_1^2\mu_2 - 3\mu_1^4}{\left(\mu_2 - \mu_1^2\right)^2} - 3, \end{aligned} \tag{24}$$

in which μ_k denotes the k-th moment given in (19) and the -3 term results to the value of zero for Gaussian distribution.

For low values of the kurtosis (e.g., close to one), the PDF is called platykurtic (i.e., $K_r < 0$), whereas it is called leptokurtic (i.e., $K_r > 0$) for high values. Note that leptokurtic RVs typically have a spiky PDF with heavy tails. In other words, the higher the kurtosis, the lower the concentration around its mean.

D. SKEWNESS

The skewness in statistics characterizes the degree of asymmetry of a distribution around its mean and it is defined as [73]

$$S_k = \frac{\mathbb{E}\left[(\Gamma - \mathbb{E}[\Gamma])^3\right]}{\left(\mathbb{E}[\Gamma^2] - \mathbb{E}^2[\Gamma]\right)^{\frac{3}{2}}} = \frac{\mu_3 - 3\mu_1\mu_2 + 2\mu_1^3}{\left(\mu_2 - \mu_1^2\right)^{\frac{3}{2}}}. \tag{25}$$

It is recalled that for symmetric statistical distributions, $S_k = 0$. Otherwise, if $S_k > 0$, the distribution is skewed to the right, and if $S_k < 0$, the distribution is skewed to the left.

Table 2 lists the values of K_r and S_k metrics for average SNR $\bar{\gamma} = 0$ dB, $N = 2$ and for different values of m and m_s. Evidently, as m and/or m_s increase(s), K_r and S_k decreases.

$$F_\Gamma(\gamma) = \frac{\text{G}_{N+1,N+1}^{N,N+1}\left[\frac{\gamma}{\bar{\gamma}}\prod_{\ell=1}^{N}\left(\frac{m_\ell}{(m_{s_\ell}-1)}\right)\middle| \begin{matrix} 1-m_{s_1}, 1-m_{s_2}, \ldots, 1-m_{s_N}, 1 \\ m_1, m_2, \ldots, m_N, 0 \end{matrix}\right]}{\prod_{\ell=1}^{N}\Gamma(m_\ell)\Gamma(m_{s_\ell})}. \tag{17}$$

TABLE 2. Values of K_r and S_k for Different Values of m and m_s with $N = 2$, and $\bar{\gamma} = 0$ dB.

Metric	m	m_s				
		5	7.5	10	20	50
K_r	2	682	100.76	56.63	28.85	20.55
	4	357.28	52.32	28.53	13.4	8.85
	6	275.88	40.01	21.35	9.42	5.82
	8	239.97	34.55	18.15	7.64	4.46
	10	219.92	31.500	16.36	6.64	3.70
S_k	2	10.39	5.99	4.89	3.79	3.31
	4	7.87	4.43	3.54	2.62	2.20
	6	7.06	3.91	3.08	2.20	1.79
	8	6.66	3.66	2.85	1.99	1.57
	10	6.43	3.50	2.71	1.85	1.43

Additionally, it is observed that as N increases, then K_r and S_k increase and their values are independent of the value of the average SNR $\bar{\gamma}$.

E. OUTAGE PROBABILITY (OP)

It is recalled that the OP is defined as the probability that the instantaneous output SNR γ falls below a certain specified threshold γ_{th}, that is

$$P_{\text{out}} = \Pr[0 \leq \gamma \leq \gamma_{\text{th}}] = \int_0^{\gamma_{\text{th}}} f_\Gamma(\gamma) d\gamma = F_\Gamma(\gamma_{\text{th}}). \quad (26)$$

Since $F_\Gamma(\gamma)$ is given in (17), the OP of the considered model is readily obtained by substituting γ with γ_{th}.

F. AVERAGE CHANNEL CAPACITY

The average channel capacity can be obtained by averaging the capacity of an AWGN channel $C_{AWGN} = W \log_2(1+\gamma)$ over the statistics of the instantaneous received SNR γ [2], that is

$$\begin{aligned} C_{\mathcal{F}} &= W \int_0^\infty \log_2(1+\gamma) f_\Gamma(\gamma) d\gamma \\ &= \frac{W}{\ln(2)} \int_0^\infty \ln(1+\gamma) f_\Gamma(\gamma) d\gamma, \end{aligned} \quad (27)$$

in which W represents the bandwidth of the fading channel.

Substituting (15) into (27), the latter can be rewritten as (28), at the bottom of the next page. To this effect and with the aid of [63, Eq. (3.4.6.5)], [63, Eq. (2.24.1.1)], and [63, Eq. (8.2.2.14)], the average capacity can be obtained as (29), at the bottom of the next page .

G. AVERAGE BIT ERROR PROBABILITY (BEP)

It is recalled that the average BEP, $\overline{P}_b$, of a digital communication system can be evaluated using

$$\overline{P}_b = \int_0^\infty P_e(\gamma) f_\Gamma(\gamma) d\gamma, \quad (30)$$

in which $P_e(\gamma)$ denotes the conditional error probability. The generic expressions of $P_e(\gamma)$ for different sets of modulation schemes [2], [74] are given below.

TABLE 3. Values of a and b in (31) for different binary modulation schemes.

Constellation	a	b
BPSK	1	$\frac{1}{2}$
DBPSK	1	1
BFSK	$\frac{1}{2}$	$\frac{1}{2}$
NBFSK	$\frac{1}{2}$	1

TABLE 4. Values of τ_M, a_M, and b_k in (34) for different constellations.

Constellation	τ_M	a_M	b_k
M-QAM	$\frac{\sqrt{M}}{2}$	$\frac{2}{\log_2 M}\left(1-\frac{1}{\sqrt{M}}\right)$	$\frac{3\log_2(M)}{2(M-1)}(2k-1)^2$
M-PSK	$\max\left(\frac{M}{4}, 1\right)$	$\frac{1}{\max(\log_2 M, 2)}$	$\log_2(M)\sin^2\frac{(2k-1)}{M}\pi$

1) BINARY MODULATIONS

For binary modulations, $P_e(\gamma)$ is given by [2, Eq. (8.100)]

$$P_e(\gamma) = \frac{1}{2\Gamma(b)} \Gamma(b, a\gamma), \quad (31)$$

in which $\Gamma(\cdot,\cdot)$ is the complementary incomplete gamma function [62, Eq. (8.350.2)], whereas, a and b are modulation-dependent parameters given in Table 3.

Now, plugging (15) and (31) into (30) yields (32), on the bottom of the next page.

Based on the above, the average BEP in (32) can be obtained, after using [63, Eq. (8.4.16.2)], [63, Eq. (2.24.1.1)], and [63, Eq. (8.2.2.14)], as in (33), on the bottom of the next page.

2) M-ARY MODULATIONS

For M-ary quadrature phase shift keying (M-PSK) and M-ary quadrature amplitude modulation (M-QAM), the conditional error probability can be written as follows [74]

$$P_e(\gamma) = a_M \sum_{k=1}^{\tau_M} \text{erfc}\left(\sqrt{b_k \gamma}\right), \quad (34)$$

in which a_M, b_k, and τ_M are modulation-dependent parameters depicted in Table 4.

Inserting (15) and (34) into (30) yields (35), at the bottom of the next page. The average BEP in (35) can be obtained, after using [63, Eq. (8.4.14.2)], [63, Eq. (2.24.1.1)], and [63, Eq. (8.2.2.14)], as in (36), at the bottom of the next page.

VI. APPROXIMATION FOR THE CASCADED FISHER-SNEDECOR $\mathcal{F}$ DISTRIBUTION

This section investigates the necessary conditions for the cascaded Fisher-Snedecor $\mathcal{F}$ fading distribution to be accurately approximated by the lognormal distribution. This provides useful insights on the relationship between the two models, and the subsequent impact of their parameters on the overall system performance.

A. LOGNORMAL DISTRIBUTION APPROXIMATION

Comparing the PDF and CDF of $N*$Fisher-Snedecor $\mathcal{F}$ distribution with that of the lognormal distribution, it can be noted

that the $N*$Fisher-Snedecor $\mathcal{F}$ distribution offers favorable handling, which can lead to a tractable representation of performance metrics such as outage probability, average BER, and average capacity. Therefore, this subsection identifies the necessary conditions which must exist for the $N*$Fisher-Snedecor $\mathcal{F}$ distribution to modeled accurately by lognormal distribution.

The PDF of a lognormal RV Z can be expressed as

$$f_Z(z) = \frac{z^{-1}}{\sqrt{2\pi\sigma_\Upsilon^2}} \exp\left(-\frac{(\ln(z)-\mu_\Upsilon)^2}{2\sigma_\Upsilon^2}\right), \tag{37}$$

in which μ_Υ and σ_Υ^2 represent the corresponding mean and the variance, respectively, whereas the average SNR per symbol, $\bar{\gamma} = (E_s/N_0)\,\mathbb{E}[Z^2]$, is given by $\bar{\gamma} = \exp\left(\mu_\Upsilon + \sigma_\Upsilon^2/2\right)$.

For the $N*$Fisher-Snedecor $\mathcal{F}$ RV, X, to be approximated by a lognormal RV, Z, a third RV is defined as

$$\Upsilon = \ln(X) = \sum_{\ell=1}^{N} \ln(R_\ell). \tag{38}$$

Note that for large values of N and by applying the CLT, Υ tends towards the normal (Gaussian) distribution, and thus, X tends to follow a lognormal distribution [75, pp. 220–221]. A necessary condition for $X \equiv Z$ is that both X and Z should have the same mean and variance, that is

$$\mu_\Upsilon = \mathbb{E}[\ln(X)], \tag{39}$$

and

$$\sigma_\Upsilon^2 = \mathbb{E}[\ln^2(X)] - \mathbb{E}[\ln(X)]^2, \tag{40}$$

in which $\mathbb{E}[\ln^2(X)]$ and $\mathbb{E}[\ln(X)]$ are defined as

$$\mathbb{E}[\ln^2(X)] = \mathbb{E}[\ln^2(R_\ell)] = \int_0^\infty \ln^2(r) f_{R_\ell}(r)dr \tag{41}$$

and

$$\mathbb{E}[\ln(X)] = \mathbb{E}[\ln(R_\ell)] = \int_0^\infty \ln(r) f_{R_\ell}(r)dr. \tag{42}$$

Using (3), the integral in (41) can be obtained in closed-form using [76, Eq. (2.6.3.10)] as

$$\mathbb{E}[\ln^2(X)] = \frac{1}{4}\Bigg\{\Big[\ln(\theta_\ell) + \psi(m_\ell) - \psi(m_{s_\ell})\Big]^2 + \psi'(m_\ell) + \psi'(m_{s_\ell})\Bigg\}, \tag{43}$$

$$C_{\mathcal{F}} = \int_0^\infty \frac{W\gamma^{-1}\ln(1+\gamma)\mathrm{G}_{N,N}^{N,N}\left[\frac{\gamma}{\bar{\gamma}}\prod_{\ell=1}^{N}\left(\frac{m_\ell}{(m_{s_\ell}-1)}\right)\middle|\begin{matrix}1-m_{s_1}, 1-m_{s_2}, \ldots, 1-m_{s_N}\\ m_1, m_2, \ldots, m_N\end{matrix}\right]}{\ln(2)\prod_{\ell=1}^{N}\Gamma(m_\ell)\Gamma(m_{s_\ell})} d\gamma. \tag{28}$$

$$C_{\mathcal{F}} = \frac{W}{\ln(2)\prod_{\ell=1}^{N}\Gamma(m_\ell)\Gamma(m_{s_\ell})}\mathrm{G}_{N+2,N+2}^{N+2,N+1}\left[\frac{1}{\prod_{\ell=1}^{N}\left(\frac{m_\ell}{(m_{s_\ell}-1)}\right)}\bar{\gamma}\middle|\begin{matrix}1-m_1, 1-m_2, \ldots, 1-m_N, 1, 1\\ m_{s_1}, m_{s_2}, \ldots, m_{s_N}, 1, 0\end{matrix}\right]. \tag{29}$$

$$\overline{P}_b = \int_0^\infty \frac{\gamma^{-1}\Gamma(b, a\gamma)\mathrm{G}_{N,N}^{N,N}\left[\frac{\gamma}{\bar{\gamma}}\prod_{\ell=1}^{N}\left(\frac{m_\ell}{(m_{s_\ell}-1)}\right)\middle|\begin{matrix}1-m_{s_1}, 1-m_{s_2}, \ldots, 1-m_{s_N}\\ m_1, m_2, \ldots, m_N\end{matrix}\right]}{2\Gamma(b)\prod_{\ell=1}^{N}\Gamma(m_\ell)\Gamma(m_{s_\ell})} d\gamma. \tag{32}$$

$$\overline{P}_b = \frac{\mathrm{G}_{N+1,N+2}^{N+2,N}\left[\frac{a}{\prod_{\ell=1}^{N}\left(\frac{m_\ell}{(m_{s_\ell}-1)}\right)}\bar{\gamma}\middle|\begin{matrix}1-m_1, 1-m_2, \ldots, 1-m_N, 1\\ m_{s_1}, m_{s_2}, \ldots, m_{s_N}, 0, b\end{matrix}\right]}{2\Gamma(b)\prod_{\ell=1}^{N}\Gamma(m_\ell)\Gamma(m_{s_\ell})}. \tag{33}$$

$$\overline{P}_b = \sum_{k=1}^{\tau_M}\int_0^\infty \frac{a_M\gamma^{-1}\mathrm{erfc}\left(\sqrt{b_k\gamma}\right)\mathrm{G}_{N,N}^{N,N}\left[\frac{\gamma}{\bar{\gamma}}\prod_{\ell=1}^{N}\left(\frac{m_\ell}{(m_{s_\ell}-1)}\right)\middle|\begin{matrix}1-m_{s_1}, 1-m_{s_2}, \ldots, 1-m_{s_N}\\ m_1, m_2, \ldots, m_N\end{matrix}\right]}{\sqrt{\pi}\prod_{\ell=1}^{N}\Gamma(m_\ell)\Gamma(m_{s_\ell})} d\gamma. \tag{35}$$

$$\overline{P}_b = \frac{a_M}{\sqrt{\pi}\prod_{\ell=1}^{N}\Gamma(m_\ell)\Gamma(m_{s_\ell})}\sum_{k=1}^{\tau_M}\mathrm{G}_{N+1,N+2}^{N+2,N}\left[\frac{b_k}{\prod_{\ell=1}^{N}\left(\frac{m_\ell}{(m_{s_\ell}-1)}\right)}\bar{\gamma}\middle|\begin{matrix}1-m_1, 1-m_2, \ldots, 1-m_N, 1\\ m_{s_1}, m_{s_2}, \ldots, m_{s_N}, 0, \frac{1}{2}\end{matrix}\right]. \tag{36}$$

TABLE 5. RAD Values for $m = 3.5$, $m_s = \{2, 4, 6, 8, 10\}$, and $N = \{1, 5, 10, 15, 20, 25, 30\}$.

$m = 3.5$							
$m_s \downarrow N \rightarrow$	1	5	10	15	20	25	30
2	0.0022	4.3355×10^{-4}	1.8787×10^{-4}	1.1963×10^{-4}	1.0617×10^{-4}	1.1628×10^{-4}	1.8327×10^{-4}
4	6.8782×10^{-4}	5.8698×10^{-5}	2.1091×10^{-5}	7.9622×10^{-6}	3.4881×10^{-6}	2.7683×10^{-6}	2.0896×10^{-6}
6	0.0018	2.8384×10^{-4}	1.337×10^{-4}	7.9856×10^{-5}	4.2300×10^{-5}	2.5961×10^{-5}	2.244×10^{-5}
8	0.0031	4.9651×10^{-4}	2.4025×10^{-4}	1.5330×10^{-4}	9.2510×10^{-5}	5.4269×10^{-5}	4.0886×10^{-5}
10	0.0042	6.6514×10^{-4}	3.2390×10^{-4}	2.1114×10^{-4}	1.3609×10^{-4}	8.1736×10^{-5}	5.6858×10^{-5}

TABLE 6. RAD Values for $m_s = 5$, $m = \{2, 4, 6, 8, 10\}$, and $N = \{1, 5, 10, 15, 20, 25, 30\}$.

$m_s = 5$							
$m \downarrow N \rightarrow$	1	5	10	15	20	25	30
2	0.0063	0.0011	4.6212×10^{-4}	1.9262×10^{-4}	1.5483×10^{-4}	1.2547×10^{-4}	1.0279×10^{-4}
4	6.8601×10^{-4}	7.7486×10^{-5}	3.2231×10^{-5}	1.7772×10^{-5}	8.4676×10^{-6}	4.9922×10^{-6}	4.3071×10^{-6}
6	3.7914×10^{-4}	1.9734×10^{-5}	8.9726×10^{-6}	5.9606×10^{-6}	4.4218×10^{-6}	3.1552×10^{-6}	2.2305×10^{-6}
8	8.9404×10^{-4}	1.0509×10^{-4}	5.3183×10^{-5}	3.6217×10^{-5}	2.7058×10^{-5}	1.9449×10^{-5}	1.3170×10^{-5}
10	0.0015	2.1088×10^{-4}	1.0523×10^{-4}	7.1163×10^{-5}	5.3489×10^{-5}	3.9876×10^{-5}	2.7664×10^{-5}

whereby $\theta_\ell = ((m_{s_\ell} - 1)\Omega_\ell)/m_\ell$, $\psi(\cdot)$ is the digamma function [62, Eq. (8.360.1)], and $\psi'(\cdot)$ is the first derivative of the digamma function. Also, using (3), the integral in (42), can be obtained in closed-form using [76, Eq. (2.6.3.7)] as

$$\mathbb{E}[\ln(X)] = \frac{1}{2}\Big[\ln(\theta_\ell) + \psi(m_\ell) - \psi(m_{s_\ell})\Big]. \tag{44}$$

Therefore, with the aid of (43) and the (44), the mean and the variance can be expressed in closed-form, respectively, as

$$\mu_\Upsilon = \frac{1}{2}\sum_{\ell=1}^{N}\Big[\ln(\theta_\ell) + \psi(m_\ell) - \psi(m_{s_\ell})\Big] \tag{45}$$

and

$$\sigma_\Upsilon^2 = \frac{1}{4}\sum_{\ell=1}^{N}\Big[\psi'(m_\ell) + \psi'(m_{s_\ell})\Big]. \tag{46}$$

B. RESISTOR-AVERAGE DISTANCE (RAD)

To measure the accuracy of our approximations, the RAD is employed to determine the information loss when approximating the exact PDF in (9) with the PDF in (37). It is recalled that the Kullback–Leibler (KL) divergence is widely used in information theory to measure the distance between two statistical distributions. It accounts for the average information loss or relative entropy between two PDFs [77], [78]. Owing to its geometric properties, computational and theoretical advantages, the KL distance is more preferable over other distance measures such as the Bhattacharyya and Chernoff distances. However, the KL distance has one main drawback: its lack of symmetry. Consequently, a symmetric version of the KL distance known as resistor-average distance (RAD) was proposed in [79]. Importantly, the RAD satisfies the triangle inequality and hence is a true distance metric. The RAD can be defined as

$$RAD = \left[\frac{1}{D_{KL}(f_1, f_2)} + \frac{1}{D_{KL}(f_2, f_1)}\right]^{-1}, \tag{47}$$

in which f_1 and f_2 denote the exact PDF and the approximated PDF, respectively, and $D_{KL}(\cdot,\cdot)$ is the KL distance, which is defined as follows

$$D_{KL}(f_i, f_j) = \int_{-\infty}^{\infty} f_i(x)\log\left(\frac{f_i(x)}{f_j(x)}\right)dx. \tag{48}$$

In Table 5 and Table 6, the results for RAD obtained from the exact PDF in (9) and the approximated PDF in (37) are provided. Note that Table 5 depicts the RAD values for a fixed value of the fading parameter (i.e., $m = 3.5$), while multiple values are used for $m_s = \{2, 4, 6, 8, 10\}$ and $N = \{1, 5, 10, 15, 20, 25, 30\}$. On the other hand, Table 6 depicts the RAD values for a fixed value of the shadowing parameter (i.e., $m_s = 5$), while the other values are set as, $m = \{2, 4, 6, 8, 10\}$ and $N = \{1, 5, 10, 15, 20, 25, 30\}$.

As shown in the two tables, for all the scenarios, the calculated RAD values are always less than 0.01, indicating that the approximated PDF (i.e., the lognormal distribution) provides an accurate fit to the exact PDF of the $N*$Fisher-Snedecor $\mathcal{F}$ distribution. Also, it is important to note that as N increases, the RAD value decreases, which consolidates the assumption stemming from the CLT.

VII. THE RATIO OF THE PRODUCT OF FISHER-SNEDECOR $\mathcal{F}$ VARIATES

Definition 2 (The ratio of $\frac{N_1}{N_2}$-Fisher-Snedecor $\mathcal{F}$ RV): The RV of the ratio, X, of N_1 and N_2 i.n.i.d. Fisher-Snedecor $\mathcal{F}$ RVs Y_ℓ, for $1 \le \ell \le N_1$, $Y_\ell \sim \mathcal{F}(m_\ell^{(1)}, m_{s_\ell}^{(1)}, \Omega_\ell^{(1)})$, and Z_w,

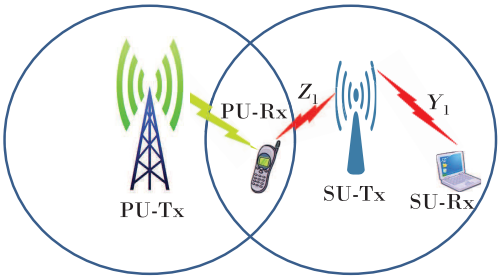

FIGURE 3. System model for spectrum sharing in CRNs.

for $1 \leq w \leq N_2$, $Z_w \sim \mathcal{F}(m_w^{(2)}, m_{s_w}^{(2)}, \Omega_w^{(2)})$, *i.e.,*

$$X = \frac{\prod_{\ell=1}^{N_1} Y_\ell}{\prod_{w=1}^{N_2} Z_w}, \tag{49}$$

is defined as the ratio of $\frac{N_1}{N_2}$*-Fisher-Snedecor* $\mathcal{F}$ *RV,* N_1 *and* $N_2 \in \mathbb{R}^+$.

Theorem 3 (Probability Density Function): The PDF of X defined in (49) can be expressed as in (50), at the top of the next page.

Proof: The PDF of X in (49) can be obtained using

$$f_X(x) = \frac{1}{x}\frac{1}{2\pi j}\oint_{\mathcal{L}} \mathbb{E}[X^s]x^{-s}ds, \tag{51}$$

where the s-th order moment of X, $\mathbb{E}[X^s]$, can be found using (49) via

$$\mathbb{E}[X^s] = \prod_{\ell=1}^{N_1} \mathbb{E}[Y_\ell^s] \prod_{w=1}^{N_2} \mathbb{E}[Z_w^{-s}]. \tag{52}$$

With the help of (7), (52), [62, Eq. (8.384.1)], and after some mathematical manipulations, the PDF of X can be expressed as in (53), at the top of the next page. Capitalizing on the definition of the Meijer's G-function in (4) and using (53), then (50) can be readily deduced, which completes the proof. ∎

Corollary 5 (Cumulative Distribution Function): The CDF of X defined in (49) can be obtained as in (54), at the top of the next page.

Proof: Using (50) and [63, Eq. (2.24.2.2)], yields (54), which completes the proof. ∎

Corollary 6 (Probability Density Function): The PDF of the instantaneous SNR Γ *can be derived as in (55), at the top of the next page.*

Proof: Using (16) and (50), yields (55), which completes the proof. ∎

Corollary 7 (Cumulative Distribution Function): The CDF of the instantaneous SNR Γ *can be obtained as in (56), at the top of the next page.*

Proof: Using (18) and (54), equation (56) is deduced, which completes the proof. ∎

VIII. PERFORMANCE ANALYSIS OF SPECTRUM SHARING NETWORKS

Consider the spectrum sharing network illustrated in Fig. 3. It is assumed that there is one primary user (PU) and one secondary user (SU). The SU transmitter (SU-Tx) can use the spectrum licensed to the PU only when the interference power at the PU receiver (PU-Rx) remains below a certain threshold. The instantaneous channel power gain from the SU-Tx to the PU-Rx is denoted by Z_1, whereas, the instantaneous channel power gain from the SU-Tx to the SU receiver (SU-Rx) is denoted by Y_1. Let Z_1 and Y_1 be independent, with channel coefficients following the Fisher-Snedecor $\mathcal{F}$ distribution, and subject to AWGN n_{z_1} and n_{y_1}, respectively. The noises n_{z_1} and n_{y_1} are assumed to be independent and circularly symmetric complex Gaussian variables with mean zero and variance N_0. It is assumed that perfect channel state information (CSI) on Z_1 and Y_1 is available at the SU-Tx. Besides, it is assumed that the interference from PU-Tx to SU-Rx can be ignored or considered in the AWGN at SU-Rx [80].

Let the instantaneous transmit power at the SU-Tx be $P(Z_1, Y_1) \geq 0$, Q_{avg} and Q_{pk} are the average and peak received power limits at the PU-Rx, respectively. Note that Q_{avg} is used to describe the long-term quality of service (QoS) at the PU-Rx, whereas Q_{pk} is used to describe the instantaneous QoS requirement. That is, $\mathbb{E}[X_1 P(Z_1, Y_1)] \geq Q_{avg}$ and $Z_1 P(Z_1, Y_1) \geq Q_{pk}$.

A. OUTAGE CAPACITY

Outage capacity (OC) is defined as the maximum rate that can be sustained with a given outage probability. Mathematically, this is equivalent to minimizing the outage probability (i.e., outage capacity) for a given transmission rate $\mathcal{R}_0$. That is

$$\begin{aligned} &\min\left\{\log_2\left(1+\frac{Y_1 P(Z_1, Y_1)}{N_0}\right) < \mathcal{R}_0\right\}, \\ &s.t.\ Z_1 P(Z_1, Y_1) \leq Q_{pk}. \end{aligned} \tag{57}$$

Since (57) is minimized for $P(Z_1, Y_1) = Q_{pk}/Z_1$, it follows that

$$P_{out} = Pr\left\{\frac{Y_1}{Z_1} < \frac{N_0(2^{\mathcal{R}_0}-1)}{Q_{pk}}\right\}, \tag{58}$$

and, thus

$$P_{out} = F_{\frac{Y_1}{Z_1}}\left(\frac{N_0(2^{\mathcal{R}_0}-1)}{Q_{pk}}\right). \tag{59}$$

With the aid of (56), the OP in (59) can be obtained as in (60), at the top of the next page. Note that $m_1^{(1)}$ and $m_{s_1}^{(1)}$ are the fading and shadowing parameters, respectively, of the target link, whereas, $m_1^{(2)}$ and $m_{s_1}^{(2)}$ are the fading and shadowing parameters, respectively, of the interfering link.

B. DELAY-LIMITED CAPACITY

The delay-limited capacity can be defined as the maximum constant transmission rate achievable over each of the fading blocks. In [80], the authors showed that the delay-limited capacity for the peak power case is zero. However, the delay-limited capacity for the average interference power Q_{avg} is

$$f_X(x) = \frac{2}{\prod_{\ell=1}^{N_1}\Gamma(m_\ell^{(1)})\Gamma(m_{s_\ell}^{(1)})\prod_{w=1}^{N_2}\Gamma(m_w^{(2)})\Gamma(m_{s_w}^{(2)})}x^{-1} \times \mathrm{G}_{N_1+N_2,N_1+N_2}^{N_1+N_2,N_1+N_2}\left[x^2\prod_{\ell=1}^{N_1}\left(\frac{m_\ell^{(1)}}{\Omega_\ell^{(1)}(m_{s_\ell}^{(1)}-1)}\right)\prod_{w=1}^{N_2}\left(\frac{\Omega_w^{(2)}(m_{s_w}^{(2)}-1)}{m_w^{(2)}}\right)\middle|\begin{matrix}1-m_{s_1}^{(1)},\ldots,1-m_{s_{N_1}}^{(1)},1-m_1^{(2)}\ldots,1-m_{N_2}^{(2)}\\ m_1^{(1)},\ldots,m_{N_1}^{(1)},m_{s_1}^{(2)},\ldots,m_{s_{N_2}}^{(2)}\end{matrix}\right]. \tag{50}$$

$$f_X(x) = \frac{1}{\prod_{\ell=1}^{N_1}\Gamma(m_\ell^{(1)})\Gamma(m_{s_\ell}^{(1)})\prod_{w=1}^{N_2}\Gamma(m_w^{(2)})\Gamma(m_{s_w}^{(2)})}\frac{1}{x}\frac{1}{2\pi j}\oint_{\mathcal{L}}x^{-s}\prod_{\ell=1}^{N_1}\Gamma(m_\ell^{(1)}+0.5s)\Gamma(m_{s_\ell}^{(1)}-0.5s) \times\left(\frac{m_\ell^{(1)}}{\Omega_\ell^{(1)}(m_{s_\ell}^{(1)}-1)}\right)^{-\frac{1}{2}s}\prod_{w=1}^{N_2}\Gamma(m_w^{(2)}-0.5s)\Gamma(m_{s_w}^{(2)}+0.5s)\times\left(\frac{\Omega_w^{(2)}(m_{s_w}^{(2)}-1)}{m_w^{(2)}}\right)^{-\frac{1}{2}s}ds. \tag{53}$$

$$F_X(x) = \frac{1}{\prod_{\ell=1}^{N_1}\Gamma(m_\ell^{(1)})\Gamma(m_{s_\ell}^{(1)})\prod_{w=1}^{N_2}\Gamma(m_w^{(2)})\Gamma(m_{s_w}^{(2)})} \times \mathrm{G}_{N_1+N_2+1,N_1+N_2+1}^{N_1+N_2,N_1+N_2+1}\left[x^2\prod_{\ell=1}^{N_1}\frac{m_\ell^{(1)}}{\Omega_\ell^{(1)}(m_{s_\ell}^{(1)}-1)}\prod_{w=1}^{N_2}\frac{\Omega_w^{(2)}(m_{s_w}^{(2)}-1)}{m_w^{(2)}}\middle|\begin{matrix}1-m_{s_1}^{(1)},\ldots,1-m_{s_{N_1}}^{(1)},1-m_1^{(2)}\ldots,1-m_{N_2}^{(2)},1\\ m_1^{(1)},\ldots,m_{N_1}^{(1)},m_{s_1}^{(2)},\ldots,m_{s_{N_2}}^{(2)},0\end{matrix}\right]. \tag{54}$$

$$f_\Gamma(\gamma) = \frac{1}{\prod_{\ell=1}^{N_1}\Gamma(m_\ell^{(1)})\Gamma(m_{s_\ell}^{(1)})\prod_{w=1}^{N_2}\Gamma(m_w^{(2)})\Gamma(m_{s_w}^{(2)})}\gamma^{-1} \times \mathrm{G}_{N_1+N_2,N_1+N_2}^{N_1+N_2,N_1+N_2}\left[\frac{\gamma}{\bar{\gamma}}\prod_{\ell=1}^{N_1}\left(\frac{m_\ell^{(1)}}{(m_{s_\ell}^{(1)}-1)}\right)\prod_{w=1}^{N_2}\left(\frac{(m_{s_w}^{(2)}-1)}{m_w^{(2)}}\right)\middle|\begin{matrix}1-m_{s_1}^{(1)},\ldots,1-m_{s_{N_1}}^{(1)},1-m_1^{(2)}\ldots,1-m_{N_2}^{(2)}\\ m_1^{(1)},\ldots,m_{N_1}^{(1)},m_{s_1}^{(2)},\ldots,m_{s_{N_2}}^{(2)}\end{matrix}\right]. \tag{55}$$

$$F_\Gamma(\gamma) = \frac{1}{\prod_{\ell=1}^{N_1}\Gamma(m_\ell^{(1)})\Gamma(m_{s_\ell}^{(1)})\prod_{w=1}^{N_2}\Gamma(m_w^{(2)})\Gamma(m_{s_w}^{(2)})} \times \mathrm{G}_{N_1+N_2+1,N_1+N_2+1}^{N_1+N_2,N_1+N_2+1}\left[\frac{\gamma}{\bar{\gamma}}\prod_{\ell=1}^{N_1}\left(\frac{m_\ell^{(1)}}{(m_{s_\ell}^{(1)}-1)}\right)\prod_{w=1}^{N_2}\left(\frac{(m_{s_w}^{(2)}-1)}{m_w^{(2)}}\right)\middle|\begin{matrix}1-m_{s_1}^{(1)},\ldots,1-m_{s_{N_1}}^{(1)},1-m_1^{(2)}\ldots,1-m_{N_2}^{(2)},1\\ m_1^{(1)},\ldots,m_{N_1}^{(1)},m_{s_1}^{(2)},\ldots,m_{s_{N_2}}^{(2)},0\end{matrix}\right]. \tag{56}$$

$$P_{out} = \frac{\mathrm{G}_{3,3}^{2,3}\left[\frac{N_0(2^{\mathcal{R}_0}-1)}{Q_{pk}\bar{\gamma}}\left(\frac{m_1^{(1)}}{(m_{s_1}^{(1)}-1)}\right)\left(\frac{(m_{s_1}^{(2)}-1)}{m_1^{(2)}}\right)\middle|\begin{matrix}1-m_{s_1}^{(1)},1-m_1^{(2)},1\\ m_1^{(1)},m_{s_1}^{(2)},0\end{matrix}\right]}{\Gamma(m_1^{(1)})\Gamma(m_{s_1}^{(1)})\Gamma(m_1^{(2)})\Gamma(m_{s_1}^{(2)})}. \tag{60}$$

formulated as [80]

$$\max \left\{ \log_2 \left(1 + \frac{Y_1 P(Z_1, Y_1)}{N_0} \right) \right\}, \quad s.t.\ \mathbb{E}[Z_1 P(Z_1, Y_1)] \leq Q_{avg}. \tag{61}$$

The optimal power allocation for the above problem is given by [80]

$$P(Z_1, Y_1) = \frac{Q_{avg}}{X_2 \mathbb{E}\left[\frac{Z_1}{Y_1}\right]}. \tag{62}$$

Thus, the delay-limited capacity can be obtained via

$$\mathcal{C}_d = \log_2 \left[1 + \frac{Q_{avg}}{\mathbb{E}\left[\frac{Z_1}{Y_1}\right] N_0} \right]. \tag{63}$$

Based on the above and with the aid of (55), [63, Eq. (2.24.2.1)], [62, Eq. (8.331)], and (63), a closed-form expression for the delay-limited capacity is obtained as

$$\mathcal{C}_d = \log_2 \left[1 + \frac{\left(1 - \frac{1}{m_1^{(1)}}\right)\left(1 - \frac{1}{m_{s1}^{(1)}}\right) Q_{avg}}{\bar{\gamma} N_0} \right]. \tag{64}$$

It can be seen from (64) that the delay-limited capacity is independent of the fading and the shadowing parameters of the interfering link.

C. ERGODIC CAPACITY

It is recalled that the ergodic capacity accounts for the maximum achievable rate averaged over all the fading blocks. In the case of average interference power constraint, such a metric can be formulated as [80]

$$\max \left\{ \mathbb{E}\left[\log_2 \left(1 + \frac{Y_1 P(Z_1, Y_1)}{N_0} \right) \right] \right\}, \quad s.t.\ \mathbb{E}[Z_1 P(Z_1, Y_1)] \leq Q_{avg}. \tag{65}$$

Thus, the ergodic capacity under average interference power constraint can be obtained by [29]

$$\mathcal{C}_{erg} = W \int_{\frac{1}{\gamma_0}}^{\infty} \log_2(\gamma_0 \gamma) f_{\frac{Y_1}{Z_1}}(\gamma) d\gamma, \tag{66}$$

in which W is the total available bandwidth and $\gamma_0 = 1/(\lambda N_0 W)$. Note that λ is calculated such that the average interference power in (66) equals Q_{avg}. Also, with the aid of (55), the PDF of Y_1/Z_1 can be expressed as in (67), as shown at the bottom of the next page. Substituting (67) into (66), yields (68), as shown at the bottom of the next page. To the best of authors' knowledge, there is no analytical solution available in the literature for the integral in (68). In what follows, a novel exact expression for this class of integrals is derived. To this end, using the definition of the Meijer's G-function in (4), the above integral, (68), can be rewritten as in (69), as shown at the bottom of the next page. Solving the inner integral in (69) with respect to γ using [76, Eq. (2.6.3.1)] and then utilizing the identity

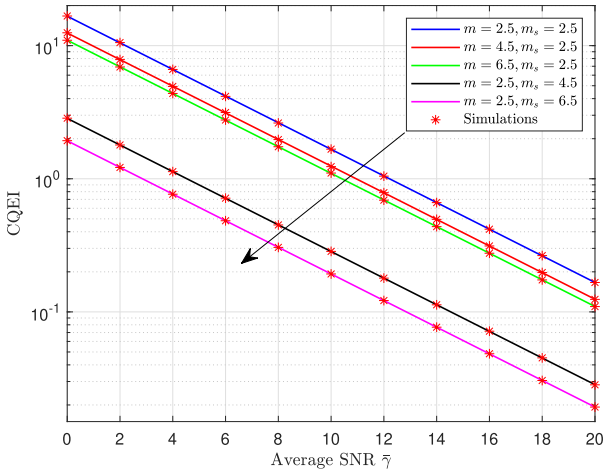

(a) $N = 2$.

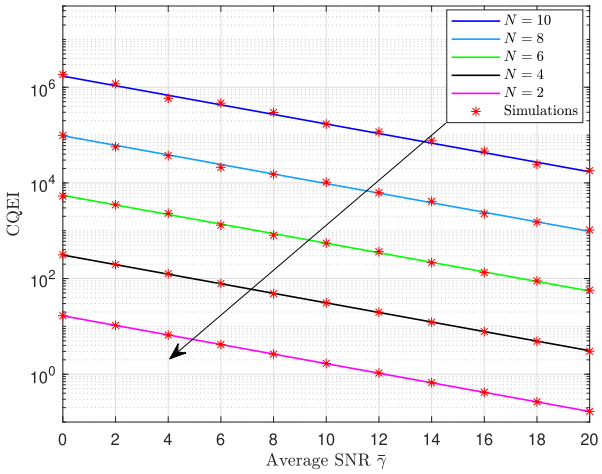

(b) $m = 2.5$, $m_s = 2.5$, and $N = 2, 4, 6, 8, 10$.

FIGURE 4. CQEI versus $\bar{\gamma}$ for i.i.d. N*Fisher-Snedecor $\mathcal{F}$ distribution.

[62, Eq. (8.331.1)] yields (70), at the bottom of the next page. Again, using the definition of Meijer's G-function, a closed-form expression for the considered ergodic capacity is derived as in (71), at the bottom of the next page.

IX. NUMERICAL RESULTS AND DISCUSSIONS

This section presents some illustrative numerical examples for the performances metrics obtained previously for both cascaded fading channels and spectrum sharing networks. Also, Monte-Carlo simulation results are provided to assess the validity of the derived analytic expressions. Importantly, very good agreement between the analytical and simulated curves is observed in all of the considered cases. Unless otherwise stated, and without loss of generality, $\mathcal{R}_0 = 1$ *bits*/*Hz* and $N_0 = 1$ *W*/*Hz*. It is noted that, in some figures, the results for the Rayleigh case are included as a benchmark.

A. CASCADED FADING CHANNELS

Fig. 4(a) and Fig. 4(b) illustrate the behavior of the CQEI as a function of the average SNR $\bar{\gamma}$. Specifically, Fig. 4(a)

shows the effect of the fading and shadowing parameters on the CQEI for $N = 2$. It is apparent that as m and (or) m_s increase(s), the CQEI decreases. This means that the system performance improves. In addition, the CQEI decreases as the average SNR $\bar{\gamma}$ increases. Note that similar behavior has been observed when altering the value of N. Fig. 4(b) shows the effect of N on the CQEI for fixed values of m and m_s. It is clear that as N increases, the CQEI also increases and as a consequence the system performance degrades.

To provide a visual interpretation of the values of the *RAD* in Table 5 and Table 6, the exact and approximated PDFs for $m = 3.5$, $m_s = 1.25$ with $N = 1$ ($RAD = 0.0088$) and $m = 6$, $m_s = 5$ with $N = 10$ ($RAD = 8.9726 \times 10^{-6}$) are provided in Fig. 5. It is clear that the lognormal distribution does not provide a good representation of the conventional Fisher-Snedecor $\mathcal{F}$ (i.e., $N = 1$) distribution. However, when $N = 10$, an excellent match is achieved. Importantly, one can note that the Rayleigh distribution provides a very poor fit to the $N*$Fisher model, as expected, as shown in Fig. 6.

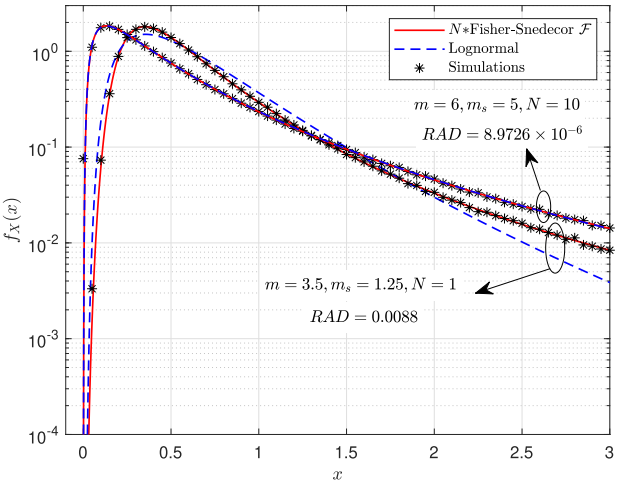

FIGURE 5. The exact PDF ($N*$Fisher-Sendecor $\mathcal{F}$) and the approximated PDF (lognormal) distributions for $m = 3.5$, $m_s = 1.25$ with $N = 1$ and $m = 6$, $m_s = 5$ with $N = 10$.

Fig. 7(a) illustrates the OP performance with $N = 4$, $m_\ell = 3.5$, and $\gamma_{th} = 0$ dB, under different shadowing conditions: $m_{s_\ell} = 1.25$ (heavy shadowing), $m_{s_\ell} = 5$ (moderate shadowing), and $m_{s_\ell} = 50$ (light shadowing), where $\ell = 1, \ldots, 4$. It can be observed that the OP improves as m_{s_ℓ} increases (i.e., the channel moves from heavy shadowing to light shadowing conditions).

Fig. 7(b) depicts the influence of N (where $N = 1, 2, 3, 4$) on the OP performance under heavy shadowing (i.e., $m_{s_\ell} = 1.25$) with fading severity $m_\ell = 3.5$ and

$$f_{\frac{Y_1}{Z_1}}(\gamma) = \frac{1}{\Gamma(m_1^{(1)})\Gamma(m_{s_1}^{(1)})\Gamma(m_1^{(2)})\Gamma(m_{s_1}^{(2)})}\gamma^{-1}\mathrm{G}_{2,2}^{2,2}\left[\frac{\gamma}{\bar{\gamma}}\left(\frac{m_1^{(1)}}{(m_{s_1}^{(1)}-1)}\right)\left(\frac{(m_{s_1}^{(2)}-1)}{m_1^{(2)}}\right)\middle|\begin{matrix}1-m_{s_1}^{(1)}, 1-m_1^{(2)}\\ m_1^{(1)}, m_{s_1}^{(2)}\end{matrix}\right]. \tag{67}$$

$$\mathcal{C}_{erg} = \frac{W}{\Gamma(m_1^{(1)})\Gamma(m_{s_1}^{(1)})\Gamma(m_1^{(2)})\Gamma(m_{s_1}^{(2)})}\int_{\frac{1}{\gamma_0}}^{\infty}\frac{\log_2(\gamma_0\gamma)\mathrm{G}_{2,2}^{2,2}\left[\frac{\gamma}{\bar{\gamma}}\left(\frac{m_1^{(1)}}{(m_{s_1}^{(1)}-1)}\right)\left(\frac{(m_{s_1}^{(2)}-1)}{m_1^{(2)}}\right)\middle|\begin{matrix}1-m_{s_1}^{(1)}, 1-m_1^{(2)}\\ m_1^{(1)}, m_{s_1}^{(2)}\end{matrix}\right]}{\gamma}d\gamma. \tag{68}$$

$$\mathcal{C}_{erg} = \frac{W}{\Gamma(m_1^{(1)})\Gamma(m_{s_1}^{(1)})\Gamma(m_1^{(2)})\Gamma(m_{s_1}^{(2)})\ln(2)}\frac{1}{2\pi j}\oint_{\mathcal{L}}\Gamma(m_1^{(1)}+s)\Gamma(m_{s_1}^{(2)}+s)\Gamma(m_{s_1}^{(1)}-s)\Gamma(m_1^{(2)}-s)$$
$$\times\left(\left(\frac{m_1^{(1)}}{(m_{s_1}^{(1)}-1)}\right)\left(\frac{(m_{s_1}^{(2)}-1)}{m_1^{(2)}}\right)\frac{1}{\bar{\gamma}}\right)^{-s}\int_{\frac{1}{\gamma_0}}^{\infty}\gamma^{-s-1}\ln(\gamma_0\gamma)d\gamma ds. \tag{69}$$

$$\mathcal{C}_{erg} = \frac{W}{\Gamma(m_1^{(1)})\Gamma(m_{s_1}^{(1)})\Gamma(m_1^{(2)})\Gamma(m_{s_1}^{(2)})\ln(2)}\frac{1}{2\pi j}\oint_{\mathcal{L}}\Gamma(m_1^{(1)}+s)\Gamma(m_{s_1}^{(2)}+s)\Gamma(m_{s_1}^{(1)}-s)\Gamma(m_1^{(2)}-s)$$
$$\times\frac{\Gamma(s)\Gamma(s)}{\Gamma(s+1)\Gamma(s+1)}\left(\left(\frac{m_1^{(1)}}{(m_{s_1}^{(1)}-1)}\right)\left(\frac{(m_{s_1}^{(2)}-1)}{m_1^{(2)}}\right)\frac{1}{\bar{\gamma}\gamma_0}\right)^{-s}ds. \tag{70}$$

$$\mathcal{C}_{erg} = \frac{W}{\Gamma(m_1^{(1)})\Gamma(m_{s_1}^{(1)})\Gamma(m_1^{(2)})\Gamma(m_{s_1}^{(2)})\ln(2)}\mathrm{G}_{4,4}^{4,2}\left[\frac{1}{\bar{\gamma}\gamma_0}\left(\frac{m_1^{(1)}}{(m_{s_1}^{(1)}-1)}\right)\left(\frac{(m_{s_1}^{(2)}-1)}{m_1^{(2)}}\right)\middle|\begin{matrix}1-m_{s_1}^{(1)}, 1-m_1^{(2)}, 1, 1\\ m_1^{(1)}, m_{s_1}^{(2)}, 0, 0\end{matrix}\right]. \tag{71}$$

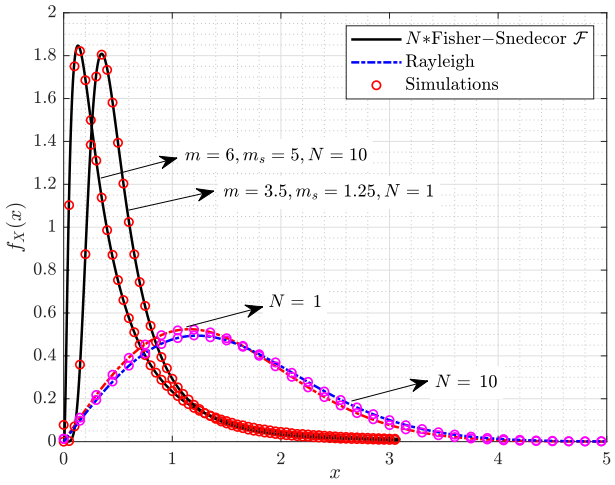

FIGURE 6. The exact PDF (N∗Fisher-Sendecor $\mathcal{F}$) and the approximated PDF (Rayleigh) distributions for $m = 3.5$, $m_s = 1.25$ with $N = 1$ and $m = 6$, $m_s = 5$ with $N = 10$.

$\gamma_{th} = 0\ dB$. It is clear that as the number of cascaded fading channels decreases, the OP performance improves substantially. For example, when $N = 1$ the required average SNR, to achieve an outage performance of 2×10^{-3}, is about 30 dB, whereas, around 18 dB ($N = 4$) to achieve the same outage performance. However, for the Rayleigh case, the same outage performance can be achieved when the average SNR is approximately 27 dB.

The impact of the fading parameter, i.e., $m_\ell = 0.5, 1, 1.5, 2$, on the OP performance is illustrated in Fig. 8 for $N = 1, 2$, $\gamma_{\text{th}} = 0$ dB, and $m_{s_\ell} = 50$ (light shadowing). The results clearly show that when the fading parameter increases, the OP performance significantly improves. This is due to the fact that when the fading parameter increases, the fading severity of the cascaded channels decreases, and hence the deep fades generated by the product of Fisher-Snedecor $\mathcal{F}$ fading envelopes occur less frequently. In Fig. 8(b), the average bit error probability performance for 4-QAM for N∗Fisher-Snedecor $\mathcal{F}$ channels with $N = 2$ and 4 under different shadowing conditions (i.e., heavy, moderate, and light) is depicted. As expected, the average bit error probability improves as the number of cascaded channels decreases. In addition, better average bit error probability performance is achieved when shadowing becomes lighter, i.e., when m_{s_ℓ} decreases. Note that similar behaviors have been noticed for the corresponding OP, in Fig. 7(a) and Fig. 7(b).

The normalized average channel capacity $C_{\mathcal{F}}/W$ under optimal rate adaptation is depicted in Fig. 9 against the average SNR $\bar{\gamma}$ with $N = 4$ under different fading severity ($m = 1.5$ (high), 3.5 (moderate)) and shadowing ($m_s = 1.25$ (heavy), 50 (light)) conditions. The results indicate that the higher the value of fading severity or/and the value of shadowing, the higher the achieved capacity. Furthermore, it is noted that the effect of shadowing is more pronounced than that of multipath fading, which verifies the need for accurate characterization of the concurrent occurrence of these two phenomena.

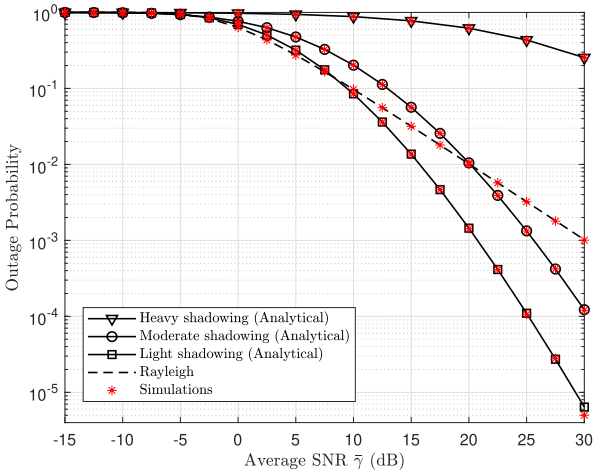

(a) $N = 4$ under different shadowing conditions for $m_\ell = 3.5$ and $\gamma_{\text{th}} = 0$ dB.

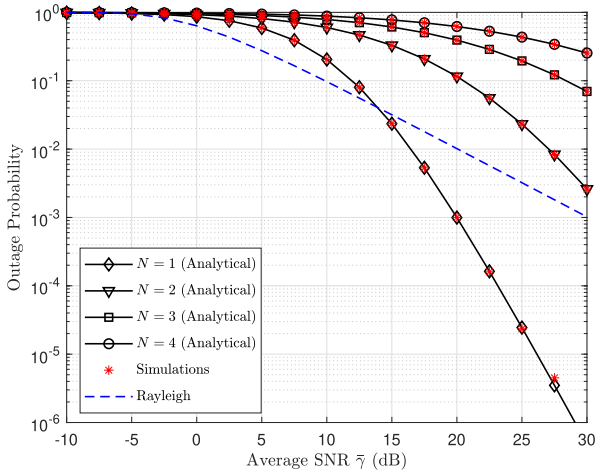

(b) $N = \{1, 2, 3, 4\}$ with heavy shadowing for $m_\ell = 3.5$ and $\gamma_{\text{th}} = 0$ dB.

FIGURE 7. OP performance as a function of average SNR $\bar{\gamma}$.

B. SPECTRUM SHARING NETWORK

Fig. 10(a) explores the influence of the peak interference power constraint Q_{pk} on the OP performance for $\mathcal{R}_0 = 1$ bits/Hz, $N_0 = 1$ W/Hz, fixed fading conditions, i.e., $m = [2.5, 2.5]$, and different shadowing conditions namely, light ($m_s = 50$) and moderate ($m_s = 5$) shadowing. The figure shows that as Q_{pk} increases, the OP performance improves. As Q_{pk} increases, this provides more flexibility to the SU-TX, allowing it to transmit with higher power. Also, the results, as expected, show that better performance can be attained when both links experience light shadowing conditions.

The impact of fading (i.e, $m \in \{2.5, 3.5, 4.5\}$) and shadowing (i.e., $m_s \in \{1.25, 5, 50\}$) experienced by the target link upon the OP performance, with $Q_{pk} = 5$ dB, $\mathcal{R}_0 = 1$ bits/Hz, and $N_0 = 1$, is depicted in Fig. 10(b). It is clear that increasing

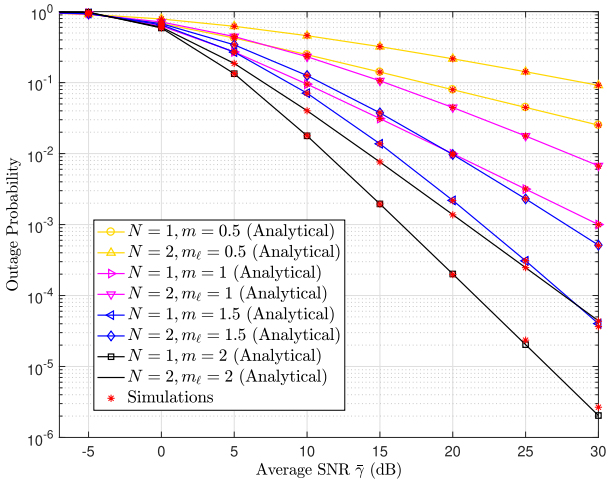

(a) OP performance as a function of average SNR $\bar{\gamma}$ with light shadowing ($m_{s_\ell} = 50$) for $N = \{1, 2\}$ and $\gamma_{\text{th}} = 0$ dB.

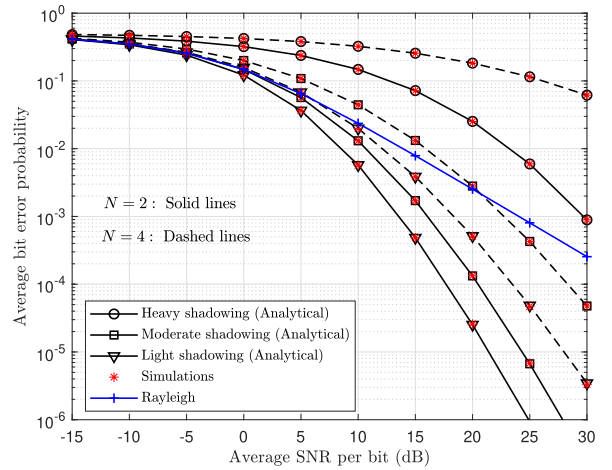

(b) Average BEP for 4-QAM performance as a function of average SNR $\bar{\gamma}$ under different shadowing conditions for $N = \{2, 4\}$ and $m_\ell = 3.5$.

FIGURE 8. **OP and Average BEP performance as a function of average SNR $\bar{\gamma}$.**

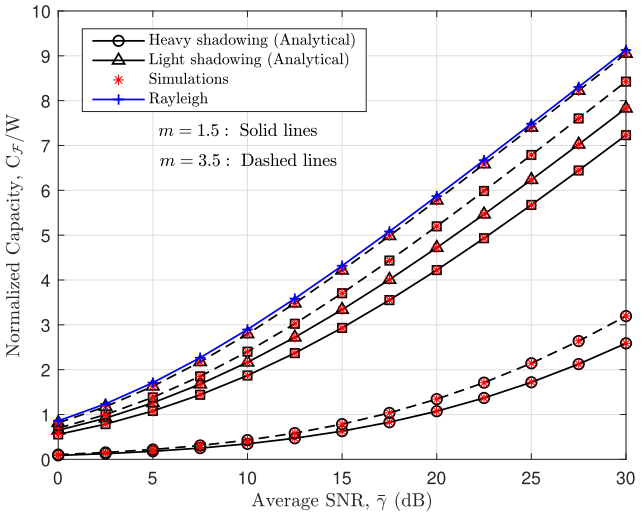

FIGURE 9. **Normalized capacity $C_{\mathcal{F}}/W$ performance as a function of average SNR $\bar{\gamma}$ for $N = 4$ under different fading and shadowing conditions.**

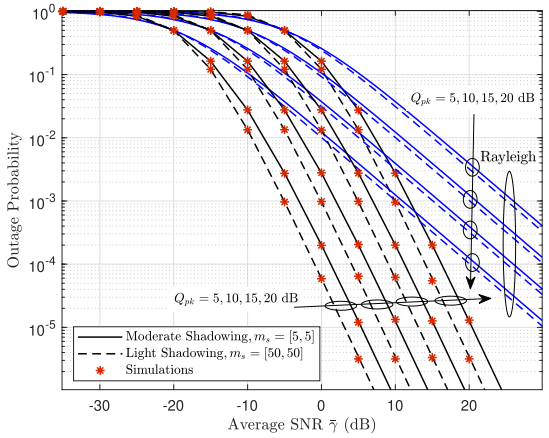

(a) Effect of peak interference power constraints under light shadowing with $m = (2.5, 2.5)$. $\mathcal{R}_0 = 1$ bits/Hz, and $N_0 = 1$ W/Hz.

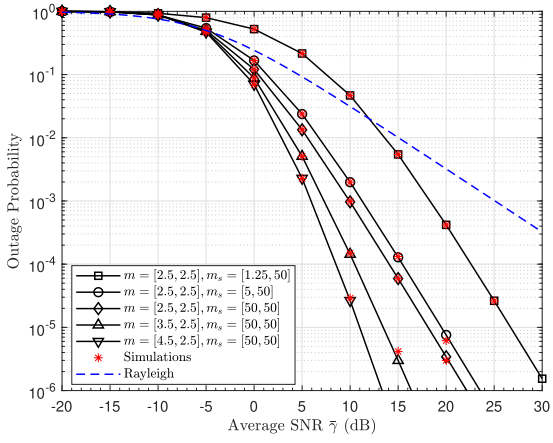

(b) Effect of fading and shadowing conditions of the target link with $Q_{pk} = 5$ dB

FIGURE 10. **OP performance, in spectrum sharing network, as a function of average SNR $\bar{\gamma}$.**

$m_1^{(1)}$ and/or $m_{s_1}^{(1)}$ decrease(s) the OP. However, the effect of $m_1^{(1)}$ on OP is more pronounced than that of $m_{s_1}^{(1)}$. On the other hand, Fig. 11(a) illustrates the influence of the fading conditions (i.e, $m \in \{0.5, 2.5, 4.5\}$) of the interfering link upon OP performance under light shadowing (i.e., $m_s = 50$) with $Q_{pk} = 5$ dB, $\mathcal{R}_0 = 1$ bits/Hz, and $N_0 = 1$. When $m_1^{(2)}$ increases, the OP performance improves. It is observed that a better OP performance, at low SNR, can be achieved when the interfering link experiences severe fading conditions (lower $m_1^{(2)}$). However, in contrast to low SNR, at high SNR the OP degrades as $m_1^{(2)}$ decreases. Also, it is noticed that as Q_{pk} becomes larger, the OP performance always improves as $m_1^{(2)}$ increases. Additionally, Fig. 10(b) and Fig. 11(a) show that the positive effect of $m_1^{(1)}$ on OP is more pronounced than that of $m_1^{(2)}$ when $m_{s_1}^{(1)}$ and $m_{s_1}^{(2)}$ are fixed. For example, when $m_{s_1}^{(1)} = m_{s_1}^{(2)} = 50$, an OP of 10^{-6} is achieved at $\bar{\gamma} = 13$ *dB* (see Fig. 10(b)) when $m_1^{(1)} = 4.5$ and $m_1^{(2)} = 2.5$. On the other hand, when $m_1^{(1)} = 2.5$ and $m_1^{(2)} = 4.5$ (see Fig. 11(a)), an OP of 10^{-6} is achieved at $\bar{\gamma} = 22$ *dB*. The effect of the shadowing

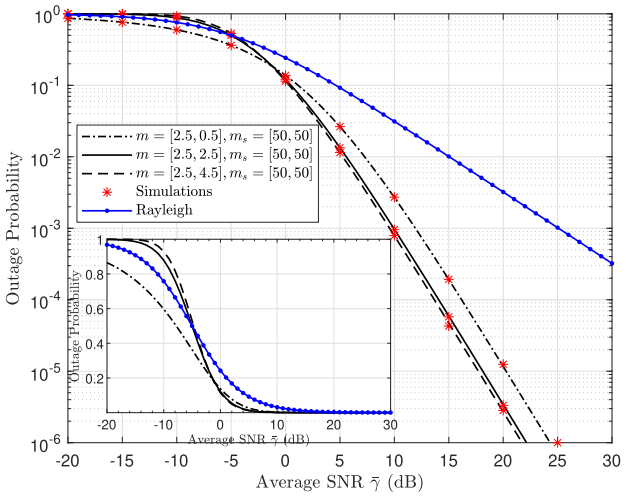

(a) Impact of fading conditions.

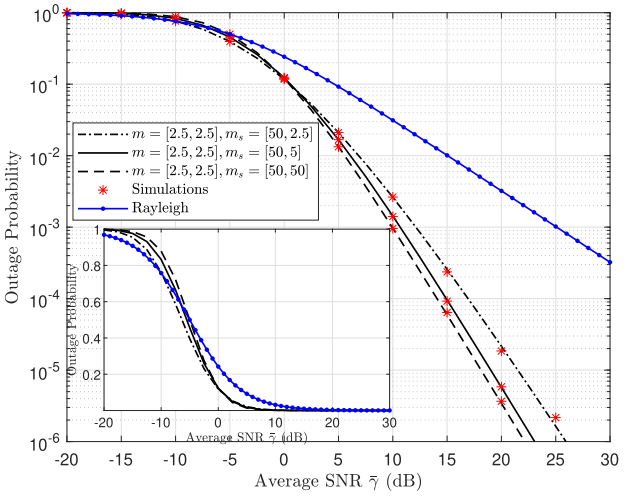

(b) Impact of shadowing conditions.

FIGURE 11. Impact of interfering link conditions on the OP performance as a function of average SNR $\bar{\gamma}$ with $Q_{pk} = 5$ dB.

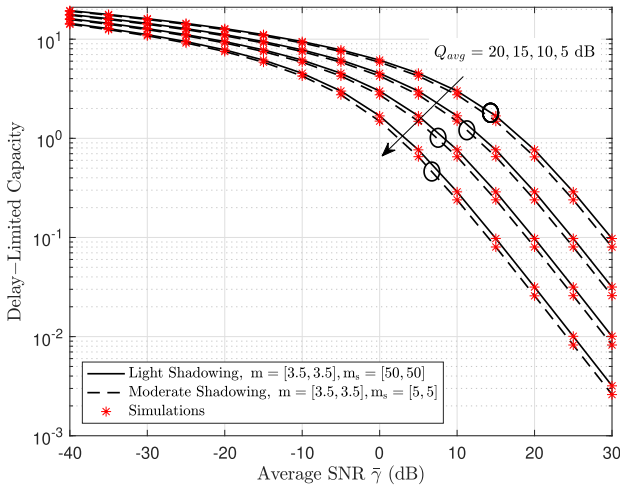

(a) Impact of the average interference power constraint Q_{avg} under moderate and light shadowing conditions.

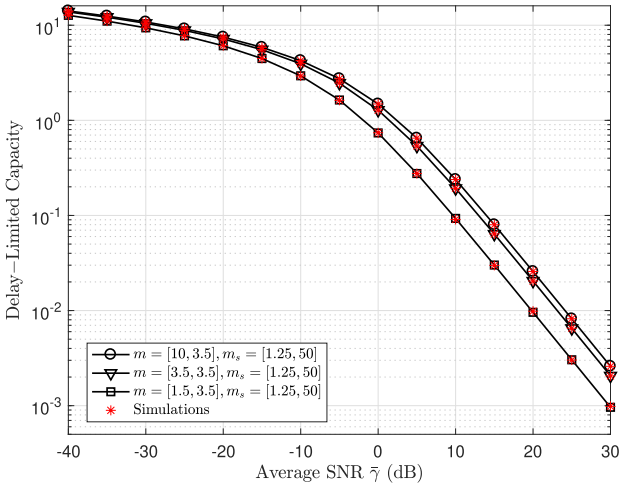

(b) Impact of fading and shadowing conditions of the target and interfering links, respectively, $Q_{avg} = 10$ dB.

FIGURE 12. Delay-limited capacity performance, in spectrum sharing network, as a function of average SNR $\bar{\gamma}$.

conditions (i.e., $m_s \in \{2.5, 5, 50\}$) of the interfering link upon OP performance, with fixed fading conditions (i.e., $m = 2.5$), $Q_{pk} = 5$ dB, $\mathcal{R}_0 = 1$ bits/Hz, and $N_0 = 1$, is illustrated in Fig. 11(b). It can be seen that better OP performance, at low SNR, can be achieved when the interfering link experiences bad shadowing conditions (lower $m_{s_1}^{(2)}$). In contrast to low SNR, at high SNR, the OP degrades as $m_{s_1}^{(2)}$ decreases.

Fig. 12(a) and Fig. 12(b) plot the delay-limited capacity performance under different scenarios. The results in Fig. 12(a) show the results for delay-limited capacity under fixed fading conditions (i.e., $m = 3.5$), different shadowing conditions (i.e., $m_s = 50$ (light), and $m_s = 5$ (moderate)), and for $Q_{avg} = 5, 10, 15, 20$ dB. It can be seen that the delay-limited capacity is improved as the average interference power constraint Q_{avg} increases. Besides, slightly better delay-limited capacity can be attained when both links experience light shadowing conditions. Fig. 12(b) shows the results for the delay-limited capacity under different fading conditions (i.e., $m \in \{1.5, 3.5, 10\}$) and shadowing conditions (i.e., $m_s = 50$ (light) and $m_s = 1.25$ (heavy)) for $Q_{avg} = 10$ dB. The results show that when $m_1^{(1)}$ increases, the delay-limited capacity increases. It is also noted that increasing/decreasing $m_1^{(2)}$ and/or $m_{s_1}^{(2)}$ has no effect on the delay-limited capacity, which is in consistent with equation (64).

Fig. 13 depicts the normalized ergodic capacity C_{erg}/W performance versus $\bar{\gamma}$ for different γ_0 (i.e., $\gamma_0 = 5, 10, 15$ dB) when both links experience similar fading conditions (i.e., $m = 3.5$) and shadowing conditions (i.e., $m_s = 50$ (i.e., light) and $m_s = 1.25$ (i.e., heavy)). It is clear that as γ_0 increases, the ergodic capacity is increased for both light and heavy shadowing conditions. However, at low SNR, better performance can be achieved when both links experience heavy shadowing conditions. It is also noticed that as the average SNR $\bar{\gamma}$ increases, the ergodic capacity becomes independent of shadowing conditions.

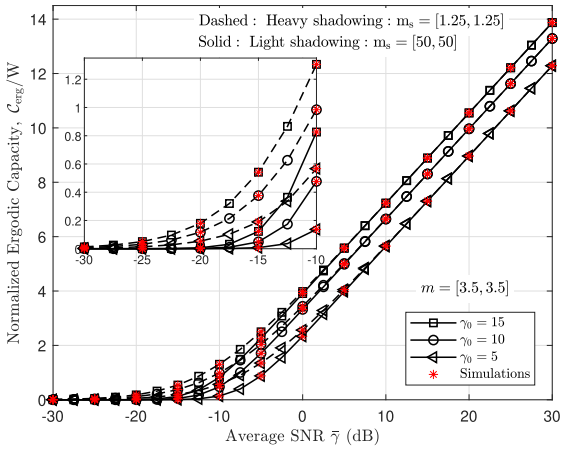

FIGURE 13. Normalized ergodic capacity C_{erg}/W performance as a function of average SNR $\bar{\gamma}$ for different γ_0 under light and heavy shadowing.

X. CONCLUSION

We have derived novel exact/closed-form expressions for several performance metrics in cascaded and spectrum sharing systems in the context of Fisher-Snedecor $\mathcal{F}$ composite fading conditions, namely the PDF, CDF and moments of the product of N $\mathcal{F}$ distributed RV and the ratio of the product of $\mathcal{F}$ distributed RV. Based on these expressions, several other metrics of interest were derived which assisted in quantifying the effect of different fading and shadowing conditions. In the case of cascaded systems: (i) for fixed values of N, m, γ_{th}, the OP performance improves with increasing values of the shadowing parameter m_s; (ii) for fixed m, m_s, and γ_{th}, the OP improves with decreasing N; (iii) for fixed shadowing conditions, γ_{th}, and N, the OP improves as the fading parameter m increases. For fixed N and m, the average BEP improves with increasing m_s, while the average BER degrades for fixed m and m_s, with increasing N. For fixed N and m_s, the average channel capacity improves with increasing m, while it decreases, for fixed N and m, with decreasing m_s. For spectrum sharing networks, when the multipath and shadowing parameters are fixed, the OP performance improves when: (i) the peak interference power constraints Q_{pk} increases; (ii) the shadowing parameter of the target link $m_{s_1}^{(1)}$ increases; (iii) at low SNR, the shadowing parameter of the interfering link $m_{s_1}^{(2)}$ decreases, while at high SNR, when $m_{s_1}^{(2)}$ increases; (iv) the fading parameter of the target link $m_1^{(1)}$ increases; (v) at low SNR, the fading parameter of the interfering link $m_1^{(2)}$ decreases, while at high SNR, when $m_1^{(2)}$ increases. In addition, when the other parameters are fixed, the delay-limited capacity increases when the average interference power constraints Q_{avg}, $m_1^{(1)}$, and(or) $m_{s_1}^{(1)}$ increase(s). Note that the delay-limited capacity is independent of fading and shadowing parameters of the interfering link (i.e, $m_1^{(2)}$ and $m_{s_1}^{(2)}$). The ergodic capacity, when both links experience similar fading and shadowing condition, improves as the shadowing parameters decrease at low SNR. However, after a certain threshold of $\bar{\gamma}$, the ergodic capacity becomes independent on shadowing parameters. Additionally, the normalized ergodic capacity improves when the values of fading and shadowing parameters of the target link increase, while it improves when the values of fading and shadowing parameters of the interfering link decrease.

ACKNOWLEDGMENT

This article was presented in part at the IEEE WiMob 2018, Limassol, Cyprus.

REFERENCES

[1] O. S. Badarneh, S. Muhaidat, P. C. Sofotasios, S. L. Cotton, K. Rabie, and D. B. da Costa, "The N* Fisher-Snedecor F cascaded fading model," in *Proc. IEEE WiMob*, Oct. 2018, pp. 1–7.

[2] M. K. Simon and M.-S. Alouini, *Digital Communications Over Fading Channels*. New York, NY, USA: Wiley, 2005.

[3] M. Nakagami, "The *m*-distribution—A general formula of intensity distribution of rapid fading," in *Statistical Methods in Radio Wave Propagation*, W. Hoffman, Ed. New York, NY, USA: Pergamon, 1960, pp. 3–36.

[4] M. Yacoub, "The κ-μ distribution and the η-μ distribution," *IEEE Antennas Propag. Mag.*, vol. 49, no. 1, pp. 68–81, Feb. 2007.

[5] M. D. Yacoub, "The α-μ distribution: A physical fading model for the Stacy distribution," *IEEE Trans. Veh. Technol.*, vol. 56, no. 1, pp. 27–34, Jan. 2007.

[6] A. Abdi and M. Kaveh, "*K* distribution: An appropriate substitute for Rayleigh-Lognormal distribution in fading-shadowing wireless channels," *IET Electron. Lett.*, vol. 34, no. 9, pp. 581–582, 1998.

[7] J. F. Paris, "Statistical characterization of $\kappa-\!-\mu$ shadowed fading," *IEEE Trans. Veh. Technol.*, vol. 63, no. 2, pp. 518–526, Feb. 2014.

[8] P. C. Sofotasios and S. Freear, "On the κ-μ/gamma composite distribution: A generalized multipath/shadowing fading model," in *IEEE MTT-S Int. Microw. Symp. Dig.*, Nov. 2011, pp. 390–394.

[9] P. C. Sofotasios and S. Freear, "The κ-μ/gamma composite fading model," in *Proc. IEEE Int. Conf. Wireless Inf. Technol. Syst.*, Sep. 2010, pp. 1–4.

[10] O. S. Badarneh, "Performance evaluation of wireless communication systems over composite α-μ/gamma fading channels," *Wireless Pers. Commun.*, vol. 97, no. 1, pp. 1235–1249, 2017.

[11] S. K. Yoo, S. L. Cotton, P. C. Sofotasios, M. Matthaiou, M. Valkama, and G. K. Karagiannidis, "The κ-μ/inverse gamma fading model," in *Proc. IEEE 26th Annu. Int. Symp. Pers., Indoor, Mobile Radio Commun. (PIMRC)*, Aug. 2015, pp. 425–429.

[12] S. Ki Yoo, P. C. Sofotasios, S. L. Cotton, M. Matthaiou, M. Valkama, and G. K. Karagiannidis, "The κ-μ/inverse gamma composite fading model," in *Proc. IEEE 26th Annu. Int. Symp. Pers., Indoor, Mobile Radio Commun. (PIMRC)*, Sep. 2015, pp. 166–170.

[13] F. Yilmaz and M. Alouini, "Extended generalized-K (EGK): A new simple and general model for composite fading channels," *CoRR*, vol. abs/1012.2598, pp. 1–27, Dec. 2010. [Online]. Available: http://arxiv.org/abs/1012.2598

[14] B. Zhu, "Asymptotic performance of composite lognormal-*X* fading channels," *IEEE Trans. Commun.*, vol. 66, no. 12, pp. 6570–6585, Dec. 2018.

[15] P. C. Sofotasios and S. Freear, "The κ-μ BC; extreme/gamma distribution: A physical composite fading model," in *Proc. IEEE Wireless Commun. Netw. Conf. (WCNC)*, Mar. 2011, pp. 1398–1401.

[16] P. C. Sofotasios and S. Freear, "On the η-μ/gamma and the λ-μ/gamma multipath/shadowing distributions," in *Proc. ATNAC*, Nov. 2011, pp. 1–6.

[17] P. C. Sofotasios, T. A. Tsiftsis, M. Ghogho, L. R. Wilhelmsson, and M. Valkama, "The η-μ/IG distribution: A novel physical multipath/shadowing fading model," in *Proc. IEEE Int. Conf. Commun. (ICC)*, Jun. 2013, pp. 5715–5719.

[18] P. C. Sofotasios, T. A. Tsiftsis, K. H. Van, S. Freear, L. R. Wilhelmsson, and M. Valkama, "The κ-μ/IG composite statistical distribution in RF and FSO wireless channels," in *Proc. IEEE 78th Veh. Technol. Conf. (VTC Fall)*, Sep. 2013, pp. 1–5.

[19] S. K. Yoo, S. L. Cotton, P. C. Sofotasios, and S. Freear, "Shadowed fading in indoor off-body communication channels: A statistical characterization using the $\kappa-\mu$/Gamma composite fading model," *IEEE Trans. Wireless Commun.*, vol. 15, no. 8, pp. 5231–5244, Aug. 2016.

[20] S. K. Yoo, N. Bhargav, S. L. Cotton, P. C. Sofotasios, M. Matthaiou, M. Valkama, and G. K. Karagiannidis, "The κ-μ/inverse gamma and κ-μ/inverse gamma composite fading models: Fundamental statistics and empirical validation," *IEEE Trans. Commun.*, early access, Dec. 6, 2019, doi: 10.1109/TCOMM.2017.2780110.

[21] G. K. Karagiannidis, N. C. Sagias, and P. Takis Mathiopoulos, "$N*$nakagami: A novel stochastic model for cascaded fading channels," *IEEE Trans. Commun.*, vol. 55, no. 8, pp. 1453–1458, Aug. 2007.

[22] I. Trigui, A. Laourine, S. Affes, and A. Stephenne, "On the performance of cascaded generalized k fading channels," in *Proc. IEEE Global Telecommun. Conf. (GLOBECOM)*, Nov. 2009, pp. 1–5.

[23] F. Yilmaz and M.-S. Alouini, "Product of the powers of generalized Nakagami-m variates and performance of cascaded fading channels," in *Proc. IEEE Global Telecommun. Conf. (GLOBECOM)*, Nov. 2009, pp. 1–8.

[24] N. C. Sagias and G. S. Tombras, "On the cascaded Weibull fading channel model," *J. Franklin Inst.*, vol. 344, no. 1, pp. 1–11, Jan. 2007.

[25] Y. Alghorani, G. Kaddoum, S. Muhaidat, S. Pierre, and N. Al-Dhahir, "On the performance of multihop-intervehicular communications systems over n^* Rayleigh fading channels," *IEEE Wireless Commun. Lett.*, vol. 5, no. 2, pp. 116–119, Apr. 2016.

[26] A.-A.-A. Boulogeorgos, P. C. Sofotasios, B. Selim, S. Muhaidat, G. K. Karagiannidis, and M. Valkama, "Effects of RF impairments in communications over cascaded fading channels," *IEEE Trans. Veh. Technol.*, vol. 65, no. 11, pp. 8878–8894, Nov. 2016.

[27] K. Peppas, F. Lazarakis, A. Alexandridis, and K. Dangakis, "Cascaded generalised-K fading channel," *IET Commun.*, vol. 4, no. 1, pp. 116–124, Jan. 2010.

[28] P. S. Bithas, A. G. Kanatas, D. B. da Costa, P. K. Upadhyay, and U. S. Dias, "On the double-generalized gamma statistics and their application to the performance analysis of V2V communications," *IEEE Trans. Commun.*, vol. 66, no. 1, pp. 448–460, Jan. 2018.

[29] E. J. Leonardo, D. B. da Costa, U. S. Dias, and M. D. Yacoub, "The ratio of independent arbitrary α-μ random variables and its application in the capacity analysis of spectrum sharing systems," *IEEE Commun. Lett.*, vol. 16, no. 11, pp. 1776–1779, Nov. 2012.

[30] O. S. Badarneh, "The α-μ/α-μ composite multipath-shadowing distribution and its connection with the extended generalized-K distribution," *AEU-Int. J. Electron. Commun.*, vol. 70, no. 9, pp. 1211–1218, Sep. 2016.

[31] O. S. Badarneh and R. Mesleh, "A comprehensive framework for quadrature spatial modulation in generalized fading scenarios," *IEEE Trans. Commun.*, vol. 64, no. 7, pp. 2961–2970, Jul. 2016.

[32] O. S. Badarneh and F. S. Almehmadi, "Performance of multihop wireless networks in α-μ fading channels perturbed by an additive generalized Gaussian noise," *IEEE Commun. Lett.*, vol. 20, no. 5, pp. 986–989, May 2016.

[33] P. C. Sofotasios, A. Bagheri, T. A. Tsiftsis, S. Freear, A. Shahzadi, and M. Valkama, "A comprehensive framework for spectrum sensing in nonlinear and generalized fading conditions," *IEEE Trans. Veh. Technol.*, vol. 66, no. 10, pp. 8615–8631, Oct. 2017.

[34] H. Al-Hmood and H. S. Al-Raweshidy, "Unified modeling of composite $\kappa-\mu$ /gamma, $\eta-\mu$/gamma, and $\alpha-\mu$/gamma fading channels using a mixture gamma distribution with applications to energy detection," *IEEE Antennas Wireless Propag. Lett.*, vol. 16, pp. 104–108, Apr. 2017.

[35] B. Zhu, J. Cheng, J. Yan, J. Wang, L. Wu, and Y. Wang, "A new asymptotic analysis technique for diversity receptions over correlated Lognormal fading channels," *IEEE Trans. Commun.*, vol. 7, no. 1, pp. 106–109, Jul. 2018.

[36] Y. Lou, Y. Zheng, J. Cheng, and H. Zhao, "Performance of SWIPT-based differential AF relaying over nakagami-m fading channels with direct link," *IEEE Wireless Commun. Lett.*, vol. 7, no. 1, pp. 106–109, Feb. 2018.

[37] H. Lei, H. Zhang, I. Shafique Ansari, Z. Ren, G. Pan, K. A. Qaraqe, and M.-S. Alouini, "On secrecy outage of relay selection in underlay cognitive radio networks over nakagami-m fading channels," *IEEE Trans. Cognit. Commun. Netw.*, vol. 3, no. 4, pp. 614–627, Dec. 2017.

[38] M. G. Kibria, G. P. Villardi, W.-S. Liao, K. Nguyen, K. Ishizu, and F. Kojima, "Outage analysis of offloading in heterogeneous networks: Composite fading channels," *IEEE Trans. Veh. Technol.*, vol. 66, no. 10, pp. 8990–9004, Oct. 2017.

[39] L. Wu, Z. Zhang, J. Dang, J. Wang, H. Liu, and Y. Wu, "Channel estimation for multicell multiuser massive MIMO uplink over Rician fading channels," *IEEE Trans. Veh. Technol.*, vol. 66, no. 10, pp. 8872–8882, Oct. 2017.

[40] E. J. Leonardo and M. D. Yacoub, "Product of α–μ Variates," *IEEE Wireless Commun. Lett.*, vol. 4, no. 6, pp. 637–640, Dec. 2015.

[41] C. R. N. da Silva, E. J. Leonardo, and M. D. Yacoub, "Product of two envelopes taken from α-μ, κ-μ, and η-μ distributions," *IEEE Trans. Commun.*, vol. 66, no. 3, pp. 1284–1295, Mar. 2018.

[42] H. Du, J. Zhang, K. P. Peppas, H. Zhao, B. Ai, and X. Zhang, "On the distribution of the ratio of products of Fisher-snedecor $\mathcal{F}$ random variables and its applications," *IEEE Trans. Veh. Technol.*, vol. 69, no. 2, pp. 1855–1866, Feb. 2020.

[43] O. S. Badarneh and D. B. da Costa, "Cascaded fluctuating two-ray fading channels," *IEEE Commun. Lett.*, vol. 23, no. 9, pp. 1497–1500, Sep. 2019.

[44] L. Kong, G. Kaddoum, and D. B. da Costa, "Cascaded $\alpha-\mu$ fading channels: Reliability and security analysis," *IEEE Access*, vol. 6, pp. 41978–41992, 2018.

[45] A.-A.-A. Boulogeorgos, P. C. Sofotasios, B. Selim, S. Muhaidat, G. K. Karagiannidis, and M. Valkama, "Effects of RF impairments in communications over cascaded fading channels," *IEEE Trans. Veh. Technol.*, vol. 65, no. 11, pp. 8878–8894, Nov. 2016.

[46] N. Hajri, N. Youssef, T. Kawabata, M. Patzold, and W. Dahech, "Statistical properties of double hoyt fading with applications to the performance analysis of wireless communication systems," *IEEE Access*, vol. 6, pp. 19597–19609, 2018.

[47] H. Shin and J. H. Lee, "Performance analysis of space-time block codes over keyhole Nakagami-m fading channels," *IEEE Trans. Veh. Technol.*, vol. 53, no. 2, pp. 351–362, Mar. 2004.

[48] M. O. Hasna and M.-S. Alouini, "Outage probability of multihop transmission over Nakagami fading channels," *IEEE Commun. Lett.*, vol. 7, no. 5, pp. 216–218, May 2003.

[49] P. N. Alevizos, K. Tountas, and A. Bletsas, "Multistatic scatter radio sensor networks for extended coverage," *IEEE Trans. Wireless Commun.*, vol. 17, no. 7, pp. 4522–4535, Jul. 2018.

[50] P. N. Alevizos, A. Bletsas, and G. N. Karystinos, "Noncoherent short packet detection and decoding for scatter radio sensor networking," *IEEE Trans. Commun.*, vol. 65, no. 5, pp. 2128–2140, May 2017.

[51] N. Fasarakis-Hilliard, P. N. Alevizos, and A. Bletsas, "Coherent detection and channel coding for bistatic scatter radio sensor networking," *IEEE Trans. Commun.*, vol. 63, no. 5, pp. 1798–1810, May 2015.

[52] C. Boyer and S. Roy, "Backscatter communication and RFID: Coding, energy, and MIMO analysis. Communications," *IEEE Trans. Commun.*, vol. 62, no. 3, pp. 770–785, Mar. 2014.

[53] K. D. Ward, C. J. Baker, and S. Watts, "Maritime surveillance radar. I. Radar scattering from the ocean surface," *IEE Proc. F, Radar Signal Process.*, vol. 137, no. 2, pp. 51–62, Apr. 1990.

[54] O. S. Badarneh, D. B. da Costa, M. Benjillali, and M.-S. Alouini, "Ratio of products of fluctuating two-ray variates," *IEEE Commun. Lett.*, vol. 23, no. 11, pp. 1944–1948, Nov. 2019.

[55] F. Graziosi and F. Santucci, "On SIR fade statistics in Rayleigh-lognormal channels," in *Proc. IEEE Int. Conf. Commun. Conf. (ICC)*, vol. 3, Apr. 2002, pp. 1352–1357.

[56] E. J. Leonardo, M. D. Yacoub, and R. A. A. de Souza, "Ratio of products of α-μ variates," *IEEE Commun. Lett.*, vol. 20, no. 5, pp. 1022–1025, May 2016.

[57] A. M. Mathai, "On products and ratios of three or more generalized gamma variables," *J. Indian Soc. Probab. Statist.*, vol. 17, no. 1, pp. 79–94, Jun. 2016.

[58] C. R. N. da Silva, N. Simmons, E. J. Leonardo, S. L. Cotton, and M. D. Yacoub, "Ratio of two envelopes taken from α-μ, η-μ, and κ-μ variates and some practical applications," *IEEE Access*, vol. 7, pp. 54449–54463, 2019.

[59] E. J. Leonardo, U. S. Dias, D. B. da Costa, and M. D. Yacoub, "Ratio of κ-μ variates and its application in spectrum sharing," in *Proc. IEEE 28th Annu. Int. Symp. Pers., Indoor, Mobile Radio Commun. (PIMRC)*, Oct. 2017, pp. 1–5.

[60] S. K. Yoo, S. L. Cotton, P. C. Sofotasios, M. Matthaiou, M. Valkama, and G. K. Karagiannidis, "The Fisher–Snedecor $\mathcal{F}$ distribution: A simple and accurate composite fading model," *IEEE Commun. Lett.*, vol. 21, no. 7, pp. 1661–1664, Jul. 2017.

[61] S. K. Yoo, P. C. Sofotasios, S. L. Cotton, S. Muhaidat, O. S. Badarneh, and G. K. Karagiannidis, "Entropy and energy detection-based spectrum sensing over $\mathcal{F}$-composite fading channels," *IEEE Trans. Commun.*, vol. 67, no. 7, pp. 4641–4653, Jul. 2019.

[62] I. S. Gradshteyn and I. M. Ryzhik, *Table of Integrals, Series, and Products*, 7th ed. New York, NY, USA: Academic, 2007.

[63] A. P. Prudnikov, Y. A. Brychkov, and O. I. Marichev, *Integrals, and Series: More Special Functions*, vol. 3. New York, NY, USA: Gordon & Breach Science, 1990.

[64] A. Mathai and R. Saxena, *The H-Function With Applications in Statiistics and Other Disciplines*. New Delhi, India: Wiley Eastern, 1978.
[65] V. Erceg, S. J. Fortune, J. Ling, A. J. Rustako, and R. A. Valenzuela, "Comparisons of a computer-based propagation prediction tool with experimental data collected in urban microcellular environments," *IEEE J. Sel. Areas Commun.*, vol. 15, no. 4, pp. 677–684, May 1997.
[66] D. Gesbert, H. Bolcskei, D. A. Gore, and A. J. Paulraj, "Outdoor MIMO wireless channels: Models and performance prediction," *IEEE Trans. Commun.*, vol. 50, no. 12, pp. 1926–1934, Dec. 2002.
[67] J. Salo, H. M. El-Sallabi, and P. Vainikainen, "Statistical analysis of the multiple scattering radio channel," *IEEE Trans. Antennas Propag.*, vol. 54, no. 11, pp. 3114–3124, Nov. 2006.
[68] A. Lioumpas, G. Karagiannidis, and A. Iossifides, "Channel quality estimation index (CQEI): A long-term performance metric for fading channels and an application in EGC receivers," *IEEE Trans. Wireless Commun.*, vol. 6, no. 9, pp. 3315–3323, Sep. 2007.
[69] T. A. Tsiftsis, F. Foukalas, G. K. Karagiannidis, and T. Khattab, "On the higher order statistics of the channel capacity in dispersed spectrum cognitive radio systems over generalized fading channels," *IEEE Trans. Veh. Technol.*, vol. 65, no. 5, pp. 3818–3823, May 2016.
[70] V. M. Rodrigo-Peñarrocha, J. Reig, L. Rubio, H. Fernández, and S. Loredo, "Analysis of small-scale fading distributions in Vehicle-to-Vehicle communications," *Mobile Inf. Syst.*, vol. 2016, pp. 1–7, Jun. 2016.
[71] J. Li, X. Cui, H. Song, Z. Li, and J. Liu, "Threshold selection method for UWB TOA estimation based on wavelet decomposition and kurtosis analysis," *EURASIP J. Wireless Commun. Netw.*, vol. 2017, no. 1, p. 202, Nov. 2017.
[72] X.-L. Liang, H. Zhang, T.-T. Lu, and T. A. Gulliver, "Threshold selection for 60 GHz TOA estimation based on skewness and kurtosis analysis," *Int. J. Smart Home*, vol. 10, no. 4, pp. 129–142, 2016.
[73] N. C. Sagias, F. I. Lazarakis, A. A. Alexandridis, K. P. Dangakis, and G. S. Tombras, "Higher order capacity statistics of diversity receivers," *Wireless Pers. Commun.*, vol. 56, no. 4, pp. 649–668, Feb. 2011.
[74] J. Lu, K. B. Letaief, J. C.-I. Chuang, and M. L. Liou, "M-PSK and M-QAM BER computation using signal-space concepts," *IEEE Trans. Commun.*, vol. 47, no. 2, pp. 181–184, Feb. 1999.
[75] A. Papoulis, *Probability, Random Variables, and Stochastic Processes*, 3rd ed. New York, NY, USA: McGraw-Hill, 1991.
[76] A. P. Prudnikov, Y. A. Brychkov, and O. I. Marichev, *Integrals, and Series: More Special Functions*, vol. 1. New York, NY, USA: Gordon & Breach Science, 1981.
[77] S. Kullback, *Information Theory and Statistics*, 1st ed. New York, NY, USA: Wiley, 1959.
[78] S. Kullback and R. A. Leibler, "On information and sufficiency," *Ann. Math. Statist.*, vol. 22, no. 1, pp. 79–86, Mar. 1951.
[79] D. H. Johnson and S. Sinanovic, "Symmetrizing the Kullback-Leibler distance," Rice Univ., Houston, TX, USA, Tech. Rep., 2001. Accessed: Nov. 22, 2020. [Online]. Available: https://scholarship.rice.edu/handle/1911/19969
[80] X. Kang, Y.-C. Liang, A. Nallanathan, H. K. Garg, and R. Zhang, "Optimal power allocation for fading channels in cognitive radio networks: Ergodic capacity and outage capacity," *IEEE Trans. Wireless Commun.*, vol. 8, no. 2, pp. 940–950, Feb. 2009.

OSAMAH S. BADARNEH (Member, IEEE) received the Ph.D. degree in electrical engineering from the École de Technologie Supérieure (ETS), University of Quebec, Canada, in 2009. From 2012 to 2018, he was an Associate Professor with the Department of Electrical Engineering, University of Tabuk. He has worked as an Assistant Professor with the Department of Telecommunication Engineering, Yarmouk University, from 2010 to 2012. He has been an Adjunct Professor with the Department of Electrical Engineering, ETS, University of Quebec, since 2013. He is currently a Professor with the Department of Electrical and Communications Engineering, German-Jordanian University. His research interest includes wireless communications and networking.

PASCHALIS C. SOFOTASIOS (Senior Member, IEEE) was born in Volos, Greece, in 1978. He received the M.Eng. degree from Newcastle University, U.K., in 2004, the M.Sc. degree from the University of Surrey, U.K., in 2006, and the Ph.D. degree from the University of Leeds, U.K., in 2011. He has held academic positions at the University of Leeds, U.K., the University of California at Los Angeles, Los Angeles, CA, USA, the Tampere University of Technology, Finland, the Aristotle University of Thessaloniki, Greece, and Khalifa University, United Arab Emirates, where he currently serves as an Assistant Professor with the Department of Electrical Engineering and Computer Science. His M.Sc. degree was funded by the Scholarship from U.K.-EPSRC and his Ph.D. degree was sponsored by U.K.-EPSRC and Pace plc. His research interests include digital and optical wireless communications and topics relating to special functions and statistics. He received the Exemplary Reviewer Award from the IEEE COMMUNICATIONS LETTERS in 2012 and the IEEE TRANSACTIONS ON COMMUNICATIONS in 2015 and 2016. He received the Best Paper Award at ICUFN 2013. He serves as a Regular Reviewer for several international journals and has been a member of the Technical Program Committee of numerous IEEE conferences. He serves as an Editor for the IEEE COMMUNICATIONS LETTERS.

SAMI MUHAIDAT (Senior Member, IEEE) received the Ph.D. degree in electrical and computer engineering from the University of Waterloo, Waterloo, ON, in 2006. From 2007 to 2008, he was an NSERC Postdoctoral Fellow with the Department of Electrical and Computer Engineering, University of Toronto, Canada. From 2008 to 2012, he was an Assistant Professor with the School of Engineering Science, Simon Fraser University, BC, Canada. He is currently a Professor with Khalifa University. His research interests include wireless communications, 5G and beyond, optical communications, the IoT with emphasis on battery-less devices, and machine learning. He has served as a Senior Editor for IEEE COMMUNICATIONS LETTERS, an Editor for IEEE TRANSACTIONS ON COMMUNICATIONS, and an Associate Editor for IEEE TRANSACTIONS ON VEHICULAR TECHNOLOGY. He is also an Area Editor of IEEE TRANSACTIONS ON COMMUNICATIONS.

SIMON L. COTTON (Senior Member, IEEE) received the B.Eng. degree in electronics and software from Ulster University, Ulster, U.K., in 2004, and the Ph.D. degree in electrical and electronic engineering from the Queen's University of Belfast, Belfast, U.K., in 2007. He was a Research Fellow, a Senior Research Fellow, a Lecturer (Assistant Professor), and a Reader (Associate Professor) with the Queen's University of Belfast, from 2007 to 2011, 2011 to 2012, 2012 to 2015, and 2015 to 2019, respectively. He is currently a Full Professor and the Director of the Centre for Wireless Innovation (CWI), Queen's University Belfast. He has authored or coauthored more than 145 publications in major IEEE/IET journals and refereed international conferences, two book chapters, and two patents. His research interests include cellular device-to-device, vehicular, and body-centric communications. His other research interests include radio channel characterization and modeling, and the simulation of wireless channels. He was awarded the H. A. Wheeler Prize, in July 2010, by the IEEE Antennas and Propagation Society for the Best Applications Journal Paper in the IEEE TRANSACTIONS ON ANTENNAS AND PROPAGATION in 2009. In July 2011, he was awarded the Sir George Macfarlane Award from the U.K. Royal Academy of Engineering in recognition of his technical and scientific attainment since graduating from his first degree in engineering.

DANIEL BENEVIDES DA COSTA (Senior Member, IEEE) was born in Fortaleza, Ceará, Brazil, in 1981. He received the B.Sc. degree in telecommunications from the Military Institute of Engineering (IME), Rio de Janeiro, Brazil, in 2003, and the M.Sc. and Ph.D. degrees in electrical engineering, area: telecommunications, from the University of Campinas, Brazil, in 2006 and 2008, respectively. From 2008 to 2009, he was a Postdoctoral Research Fellow with INRS-EMT, University of Quebec, Montreal, QC, Canada. Since 2010, he has been with the Federal University of Ceará, where he is currently an Associate Professor. He is a member of the IEEE Communications Society and the IEEE Vehicular Technology Society. His Ph.D. thesis was awarded the Best Ph.D. Thesis in Electrical Engineering by the Brazilian Ministry of Education (CAPES) at the 2009 CAPES Thesis Contest. He was a recipient of four conference paper awards. He received the Exemplary Reviewer Certificate of the IEEE Wireless Communications Letters in 2013, the Exemplary Reviewer Certificate of the IEEE Communications Letters in 2016 and 2017, the Certificate of Appreciation of Top Associate Editor for outstanding contributions to IEEE Transactions on Vehicular Technology in 2013, 2015, and 2016, the Exemplary Editor Award of IEEE Communications Letters in 2016, and the Outstanding Editor Award of IEEE Access in 2017. He has been involved on the Organizing Committee of several conferences. He is the Latin American Chapters Coordinator of the IEEE Vehicular Technology Society. He also acts as a Scientific Consultant of the National Council of Scientific and Technological Development (CNPq), Brazil, and he is a Productivity Research Fellow of CNPq. He is also the Vice-Chair of Americas of the IEEE Technical Committee of Cognitive Networks (TCCN), the Director of the TCCN Newsletter, and the Chair of the Special Interest Group on "Energy-Harvesting Cognitive Radio Networks" in IEEE Transactions on Cognitive Communications and Networking. He is also the Executive Editor of the IEEE Communications Letters and an Editor of the IEEE Communications Surveys and Tutorials, IEEE Transactions on Communications, IEEE Transactions on Vehicular Technology, IEEE Access, IEEE Transactions on Cognitive Communications and Networking, and *EURASIP Journal on Wireless Communications and Networking*. He has served as an Associate Technical Editor for *IEEE Communications Magazine*. From 2012 to 2017 and March 2019 to August 2019, he was an Editor of the IEEE Communications Letters. He has served as an Area Editor for IEEE Open Journal of the Communications Society–Area: Green, Cognitive, and Intelligent Communications and Networks, and as a Guest Editor of several Journal Special Issues. He is a Distinguished Lecturer of the IEEE Vehicular Technology Society.